


Diverse phase transitions in optimized directed network models with distinct inward and outward node weights

Rong-Chih Chang (張容誌),¹ An-Liang Cheng (鄭安良),¹ and Pik-Yin Lai (黎璧賢) ^{1,2,*}

¹*Department of Physics and Center for Complex Systems, National Central University, Chung-Li District, Taoyuan City 320, Taiwan, Republic of China*

²*Physics Division, National Center for Theoretical Sciences, Taipei 10617, Taiwan, Republic of China*



(Received 22 November 2022; accepted 7 March 2023; published 23 March 2023)

We consider growing directed network models that aim at minimizing the weighted connection expenses while at the same time favoring other important network properties such as weighted local node degrees. We employed statistical mechanics methods to study the growth of directed networks under the principle of optimizing some objective function. By mapping the system to an Ising spin model, analytic results are derived for two such models, exhibiting diverse and interesting phase transition behaviors for general edge weight, inward and outward node weight distributions. In addition, the unexplored cases of negative node weights are also investigated. Analytic results for the phase diagrams are derived showing even richer phase transition behavior, such as first-order transition due to symmetry, second-order transitions with possible reentrance, and hybrid phase transitions. We further extend previously developed zero-temperature simulation algorithm for undirected networks to the present directed case and for negative node weights, and we can obtain the minimal cost connection configuration efficiently. All the theoretical results are explicitly verified by simulations. Possible applications and implications are also discussed.

DOI: [10.1103/PhysRevE.107.034312](https://doi.org/10.1103/PhysRevE.107.034312)

I. INTRODUCTION

The availability of a large number of technological and biological data in the last two decades flourished the studies on complex networks [1–3]. At the same time, other network data such as social, internet, biodata and technical data banks, etc., become conveniently accessible through internet further enhance the research activities of complex networks. Several key issues are of particular interests, one is how the network topology affects the function of these complex networks, as in the case of biological networks. Another issue concerns the principles behind the formation or growth of such networks under some optimization goals [4,5]. This is associated with the question of network coevolution and the development or connection rules in the network are essential. Presumably a system is optimizing towards some goal or function, but subject to some constraints and regulated by feedback of the status of the network. In many cases, these goals and constraints are not constant in time but slowly varying, which is related to the problem of selection and adaptation in biology in a broad sense [6–8]. In addition, there were also efforts to understand the designing principle for network formation that optimizes information flow [9,10] or robustness against random or targeted attacks [11,12].

Recently, we have developed the basic theoretical framework for optimized network with undirected connections and investigated the drastic structural changes associated with phase transitions [13] and the network properties of the optimized undirected networks [14]. Our motivation was to

understand the relation between the cost and the connectivity in network connection growth models. The optimizing goal is to minimize the cost of connection material but at the same time trying to maximize network connections, or other relevant beneficial quantities under some possible constraints [15]. Two connection growth models of undirected network were developed in Ref. [13] and by mapping the network into an Ising spin system, it is found that the optimization of these undirected network can often be solved exactly and in many case these models exhibit interesting phase transition behaviors. Based on mean-field theories, an algorithm to search for the optimized undirected link configuration was developed and proved to be highly efficient in the zero-temperature simulations needed for the fully optimized solution.

However, one of the most important feature of a complex network is how the nodes are connected, including the strength of the connection and their directionality. As interactions or relations between nodes can be described by their directed link connections, this feature determines the overall properties and governs the dynamics and functionality of the network. A node can affect another node but itself is unaffected or affected to a different extend by the latter. Such unidirectional interactions are represented as directed networks with directional links. Examples for directed links includes the chemical synaptic connection from the presynaptic neuron to the postsynaptic neuron; master-slave interacting networks in which the master nodes can deliver output command signals to the slave nodes, but not viceversa. Presumably, the evolution or formation of such directed networks is guided by some objective function that the system tries to achieve an optimal target.

*pylai@phy.ncu.edu.tw

Unlike many previous studies relating Ising spins and networks in which each spin variable sits on a node and interacts through the network link with another spin on another node [16], in this work the Ising spin or binary variable represents the connection between two nodes [13,14,17,18]. There were some studies in which the undirected network structure is also determined by a Hamiltonian consists of binary variables representing the links [17,18]. These studies investigated the phase transition of network structure of an undirected network by re-wiring the connections (i.e., total number of edges is conserved) as the temperature is changed. In our present study, we examine the phase transitions of directed networks whose connections are free to vary at zero-temperature (no “noise” or fully optimized) as the parameters of the edge weight or node weight distributions change. In the present work, using mean-field theory approach, analytic and exact results for a variety of phase transitions are discovered and verified by simulations whereas the above mentioned works [17,18] were largely simulations or phenomenological theory.

In this paper, we extend our previous studies for the optimization of undirected network connections [13,14] and construct two models for the optimized directed networks and investigate the associated network phase transitions. We consider directed network growing models that aim at minimizing the connection expenses while at the same time enhancing other important network properties such as network connections. Directed connections lead naturally to the distinction of inward and outward node weights that can give rise to richer behavior and more diverse phase transitions for the optimized network. Classical network models and statistical mechanics methods are employed to study the growth of some networks under the principle of optimizing some objective function. By mapping the system to an Ising spin model, our analytic results indicate that these models exhibit rich and interesting phase transition behaviors, such as first-order, second-order, and reentrant phase transitions. In this paper, using the mean-field theories, we derive the zero-temperature mean-field equations for the optimized directional network connections, which further enables the development of an efficient algorithm to find the optimized directed network (ground-state) configurations. In addition, we consider the cases of negative node weights which has not been explored even for the undirected networks. A node with a negative weight means that node does not favor to have connections. Analytic results, including the optimized mean connectivity and cost, the nature of the network phase transitions and the associated transition points, the phase diagram together with the phase boundaries, are derived. Monte Carlo simulations using the proposed new algorithm are carried out to explicitly verify these analytic results.

II. DIRECTED NETWORK CONNECTION GROWING MODEL WITH EDGE AND NODE WEIGHTS

Consider the system which consists of N nodes, and the connections are described by the $N \times N$ adjacency matrix A_{ij} [see Fig. 1(a)]. The elements A_{ij} take the value of 1 or 0, respectively, for connection or no connection. Here we do not consider multiple connections between two nodes and there is no self-connection ($A_{ii} = 0$). The cost function for a general

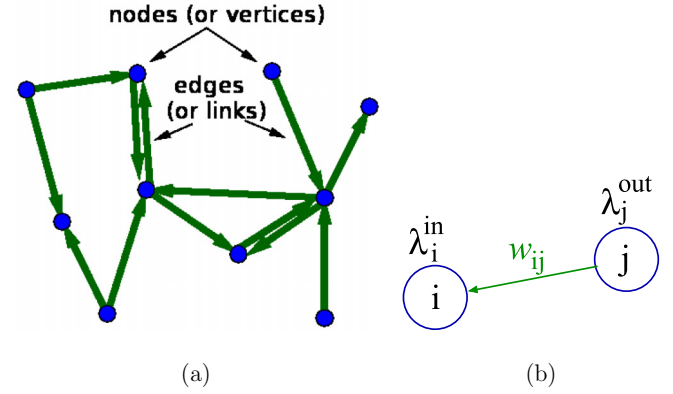


FIG. 1. (a) Schematic figure illustrating a network with directed links. (b) Picture showing a directed connection from node j to node i with an edge weight w_{ij} . The inward connection of node i is associated with an inward node weight of λ_i^{in} , and the outward connection of node j is associated with an outward node weight of λ_j^{out} .

network connection growth is modeled as

$$\mathcal{C} = \sum_{i \neq j}^N w_{ij} A_{ij} - \mathcal{F}(\{A_{ij}\}; \{\lambda_i^{\text{in}}, \lambda_i^{\text{out}}\}), \quad (1)$$

where \mathcal{F} is some function of the adjacency matrix elements to model the system’s advantage which is some quantitative measure of the benefit when the directed connections are built up. To model the local intrinsic heterogeneity or variation of each node, we further introduce two local node weights for the inward and outward connections of each node i , denoted, respectively, by λ_i^{in} and λ_i^{out} . The weight of each connection is denoted by w_{ij} which can be interpreted as the price (such as the wiring materials) to set up the connection A_{ij} . w_{ij} is taken to be nonnegative throughout this paper. Here the cost function \mathcal{C} is a function of the adjacency matrix elements whereas w_{ij} , λ_i^{in} , and λ_i^{out} are treated as parameters of the system, which are to be assumed to follow some mutually independent probability distributions denoted, respectively, by $P(w)$, $p_{\text{in}}(\lambda)$, and $p_{\text{out}}(\lambda)$. Note that w_{ij} depends on the edge whereas λ_i^{in} and λ_i^{out} are node dependent. In a directed network, there can be two oppositely directed edges between two nodes. The maximal total number of possible connections or bonds is $N_b = N(N - 1)$. For convenience, the directed edge of the network is labeled by the Greek index γ ($\gamma = 1, 2, \dots, N_b$) hereafter. Throughout this paper, it is implicitly assumed that the network is large with $N \gg 1$ and $N_b \simeq N^2$. By introducing the spin variable $S_\gamma \equiv 2A_\gamma - 1$, the system then be described by an Ising spin model with spin value $S_\gamma = 1$ (connections) or -1 (no connection). Then the problem of finding the minimal cost solution becomes the search of the ground-state configuration of the Ising spins. With the above mapping of the directed network adjacency matrix to an Ising spin system, the optimized connections or the Ising spin configurations can be obtained by the standard metropolis Monte Carlo simulation method annealed down to very low temperature for the approximate solution of the fully optimized solution (the ground state). But such traditional Monte Carlo simulations with temperature annealing becomes

inefficient and computationally demanding in searching for the zero-temperature ground-state configurations. Due to the fact that each node in the network can have different affinities of joining a directed link, i.e., the node weights for the inward and outward connections are different, the dimension of the parameter space is doubled for directed networks as compared to the undirected case, and hence allowing richer phase transition behaviors.

In this paper, by invoking mean-field theories, the mean-field equations for the fully optimized configuration (ground state) are derived and diverse phase transitions are obtained and analyzed in Sec. IV. The case of negative node weights are considered in Sec. V. And in Sec. VI, based on the zero-temperature mean-field equations, efficient algorithm is further proposed, including the scenarios of negative node weights, and implemented to obtain the fully optimized directed network configurations. Simulations using the zero-temperature algorithm are carried out, for networks with $N = 100$ to 500 nodes, to verify all the theoretical results.

III. OPTIMIZED DIRECTED NETWORKS WITH INWARD AND OUTWARD WEIGHTED NODES: MODEL A

First we consider a simpler model, which we called Model A. The cost function is modeled as

$$C_A = \sum_{i \neq j}^N w_{ij} A_{ij} - \left(\sum_{i=1}^N \lambda_i^{\text{in}} k_i^{\text{in}} + \sum_{i=1}^N \lambda_i^{\text{out}} k_i^{\text{out}} \right), \quad (2)$$

where k_i^{in} and k_i^{out} are, respectively, the in-degree and out-degree of node i . The first term in the cost function represents the resources or materials needed to set up the connections, while the second term models the trend for the network to make more connections. An example would be the formation of a neuronal network, the first term in Eq. (2) corresponds to the material or energy budget for the neural connections

$$\left\langle \frac{1}{N_b} \sum_{\alpha} S_{\alpha} \right\rangle = \frac{1}{N_b} \sum_{\alpha} \tanh \frac{\beta}{2} (\Lambda - w) \xrightarrow{N_b \rightarrow \infty} \int dw \int d\Lambda \tanh \frac{\beta}{2} (\Lambda - w) P(\Lambda, w), \quad (8)$$

where $P(\Lambda, w)$ is the joint distribution of Λ and w . Throughout this paper, we will assume the node and edge weight distributions are independent, i.e., $P(\Lambda, w) = \mathbf{P}(\Lambda)P(w)$.

From the expression of C_A in Eq. (4), one can easily deduce that the edges with $w_{\alpha} < \Lambda_{\alpha}$ should be built up to reduce the total cost of the system. In the zero-temperature limit ($\beta \rightarrow \infty$), the connection of each edge simply given by

$$A_{\alpha} = \Theta(\Lambda_{\alpha} - w_{\alpha}), \quad \alpha = 1, 2, \dots, N_b. \quad (9)$$

Hence, to obtain the configuration of the fully optimized network for Model A, one can adopt the simple rule of making connections with $\Lambda_{\alpha} > w_{\alpha}$. In terms of an Ising spin system, Eq. (9) simply means that the ground state is given by the Ising spins align with the local external fields. In addition, the mean

such as the axons and dendrites, while the second term models (for positive λ_{in} and λ_{out}) the tendency to make more neuronal connections so as to carry out efficient information or neural signal flows to achieve important biological functions. Another example is a physical network with links made of wiring material such as a circuit, the goal is to design the circuit with minimal wiring hardware materials but still can connect a large number of nodes for efficient information flow.

For directed networks, each node i is allowed to have different inward and outward local node weights, λ_i^{in} and λ_i^{out} . Defining the link dependent parameter

$$\Lambda_{\alpha} \equiv \Lambda_{ij} \equiv \lambda_i^{\text{in}} + \lambda_j^{\text{out}}, \quad (3)$$

the cost function can be simplified to

$$C_A = \sum_{\alpha=1}^{N_b} (w_{\alpha} - \Lambda_{\alpha}) A_{\alpha}. \quad (4)$$

If λ_i^{in} and λ_i^{out} follow the distribution P_{in} and P_{out} , respectively (also assumed to be independent of each other), then the distribution of Λ_{α} is given by

$$\mathbf{P}(\Lambda) = \int d\lambda P_{\text{out}}(\lambda) P_{\text{in}}(\Lambda - \lambda). \quad (5)$$

With the Ising spin variable $S_{\gamma} \equiv 2A_{\gamma} - 1$, the model can be described by the noninteracting Ising spin Hamiltonian:

$$\mathcal{H}_A = -\frac{1}{2} \sum_{\alpha=1}^{N_b} (\Lambda_{\alpha} - w_{\alpha}) S_{\alpha}. \quad (6)$$

The corresponding partition function is given by

$$\ln Z = \sum_{\alpha=1}^{N_b} \ln 2 \cosh \left[\frac{\beta}{2} (w_{\alpha} - \Lambda_{\alpha}) \right]. \quad (7)$$

The average mean connectivity is related to the order-parameter (magnetization) of the system via $2\langle \bar{A} \rangle - 1 = \langle \frac{1}{N_b} \sum_{\alpha} S_{\alpha} \rangle$ which can be calculated to give

connectivity of the optimized network is given by

$$\bar{A} = \frac{1}{N_b} \sum_{\alpha=1}^{N_b} \Theta(\Lambda_{\alpha} - w_{\alpha}) \xrightarrow{N_b \rightarrow \infty} \bar{A} = \int d\Lambda \mathbf{P}(\Lambda) F_w(\Lambda), \quad (10)$$

where F_w is the cumulative distribution of edge weight distribution $P(w)$:

$$F_w(z) = \int_{-\infty}^z P(w) dw. \quad (11)$$

Using Eq. (3), one can derive the mean connectivity of the optimized directed network in Model A to be

$$\bar{A} = \iint d\lambda_1 d\lambda_2 P_{\text{out}}(\lambda_1) P_{\text{in}}(\lambda_2) F_w(\lambda_1 + \lambda_2). \quad (12)$$

The above expression is valid when the two distributions P_{out} and P_{in} are independent.

Hereafter we shall develop the theoretical framework for describing the behavior of the optimized network for general edge and node weight distributions that depend on a single scale, one can write

$$P_{\text{in}}(\lambda) = \frac{1}{\lambda_o^{\text{in}}} p_{\text{in}}\left(\frac{\lambda}{\lambda_o^{\text{in}}}\right), \quad P_{\text{out}}(\lambda) = \frac{1}{\lambda_o^{\text{out}}} p_{\text{out}}\left(\frac{\lambda}{\lambda_o^{\text{out}}}\right), \quad (13)$$

$$P(w) = \frac{1}{w_o} p\left(\frac{w}{w_o}\right), \quad \int^w P(w)dw \equiv F_w(w) = f_w\left(\frac{w}{w_o}\right), \quad (14)$$

for some functions p_{in} , p_{out} , and p that satisfy the normalization conditions, λ_o^{in} , λ_o^{out} , and w_o are the parameters characterizing the corresponding distributions. Then the behavior of the system is governed by only two independent parameters $a \equiv \frac{\lambda_o^{\text{out}}}{w_o}$ and $b \equiv \frac{\lambda_o^{\text{in}}}{w_o}$. The finite-temperature average mean connectivity can then be written as

$$\langle \bar{A} \rangle = \frac{1}{2} \iint dr ds p_{\text{in}}(r) p_{\text{out}}(s) \times \int dw p(w) \left[1 + \tanh \frac{\beta}{2} (as + br - w) \right]. \quad (15)$$

The zero-temperature or fully optimized mean connectivity and optimized cost can be straightforwardly calculated to give

$$\begin{aligned} \bar{A} &= \iint dr ds p_{\text{in}}(r) p_{\text{out}}(s) f_w(as + br), \quad (16) \\ \frac{C_A}{N_b w_o} &= \iint dr ds p_{\text{in}}(r) p_{\text{out}}(s) \\ &\times \left[\int^{as+br} dz z p(z) - (as + br) f_w(as + br) \right]. \quad (17) \end{aligned}$$

Below we shall derive some analytical results for several given edge and node distributions and verify these results by Monte Carlo simulations.

A. Model A with homogeneous node weights

In this case, each node has the same inward weight and outward weight with $p_{\text{in}}(r) = \delta(r - 1)$ and $p_{\text{out}}(s) = \delta(s - 1)$. The finite-temperature average mean connectivity can be calculated from Eq. (15) with an exponentially distributed (nonnegative) edge weight $p(w) = e^{-w}$ ($w \in [0, \infty)$) to give

$$\langle \bar{A} \rangle = {}_2F_1\left(1, 1 + \frac{1}{\beta}; 2 + \frac{1}{\beta}; -e^{(a+b)\beta}\right) \frac{e^{(a+b)\beta}}{1 + \beta}, \quad (18)$$

where ${}_2F_1$ is the hypergeometric function. Traditional metropolis Monte Carlo simulations of the corresponding Ising spin system at finite temperature is performed and the average magnetization is measured to give $\langle \bar{A} \rangle$ as a function of the parameter $a + b$ as plotted in Fig. 2(a), verifying the formula in Eq. (18).

The optimized mean connectivity and cost can be directly obtained from Eqs. (16) and (17) to be

$$\bar{A} = f_w(a + b), \quad \frac{C_A}{N_b w_o} = \int^{a+b} dz z p(z) - (a + b) f_w(a + b). \quad (19)$$

It is clear that in this case, the properties of the optimized network depends only on a single parameter $a + b$. For an exponentially distributed (nonnegative) edge weight, $p(w) = e^{-w}$ with $w \in [0, \infty)$, Eq. (19) reads

$$\begin{aligned} \bar{A} &= [1 - e^{-(a+b)}] \Theta(a + b), \\ \times \frac{C_A}{N_b w_o} &= [1 - e^{-(a+b)} - (a + b)] \Theta(a + b) \leq 0. \quad (20) \end{aligned}$$

Zero-temperature simulations are easily carried out by using Eq. (9) to connect the link α whenever Λ_α exceeds w_α . Figure 2(a) also shows the measured \bar{A} as a function of the parameter $a + b$, showing perfect agreement with the prediction in Eq. (20).

B. Exponential distributions in node and edge weights

For exponentially distributed (nonnegative) edge and node weights, we have $p(w) = e^{-w}$, $p_{\text{in}}(r) = e^{-r}$ and $p_{\text{out}}(s) = e^{-s}$, $r, s, w \in [0, \infty)$ and the optimized mean connectivity can be obtained from Eqs. (16) and (17) as

$$\bar{A} = \frac{a + b + ab}{(1 + a)(1 + b)}, \quad \frac{C_A}{N_b w_o} = \frac{1 - a^2 - b^2 - ab(a + b)}{(1 + a)(1 + b)}. \quad (21)$$

Figure 2(b) shows the simulation results of the mean connectivity of the optimized network as a function of a for the cases of $b = a$ and $b = 1$. The corresponding theoretical results from Eq. (21) are also displayed showing perfect agreement. Figures 2(c) and 2(d) display the contour plots of \bar{A} and (normalized) C_A as a function of a and b as given by Eq. (21). The variations of the optimized mean connectivity is smooth and no phase transition occurs.

C. Equal edge weight distribution

Now each edge shares the same weights, namely $p(w) = \delta(w - 1)$. From Eqs. (16) and (17), one gets

$$\begin{aligned} \bar{A} &= \iint dr ds p_{\text{in}}(r) p_{\text{out}}(s) \Theta(as + br - 1), \quad (22) \\ \frac{C_A}{N_b w_o} &= - \iint dr ds p_{\text{in}}(r) p_{\text{out}}(s) (as + br - 1) \\ &\Theta(as + br - 1) \leq 0. \quad (23) \end{aligned}$$

For illustration, consider uniform distribution of node weights in some finite domain, namely $P_{\text{in}}(\lambda) = 1/\lambda_o^{\text{in}}$ for $\lambda \in [0, \lambda_o^{\text{in}}]$ and $P_{\text{out}}(\lambda) = 1/\lambda_o^{\text{out}}$ for $\lambda \in [0, \lambda_o^{\text{out}}]$, i.e., $p_{\text{in}}(r) = 1$ for $r \in [0, 1]$ and = 0 otherwise; and similarly for p_{out} . Using Eq. (22) and after some algebra, formula for $\bar{A}(a, b)$ can be derived whose functional form depends on the regimes in the ‘‘phase

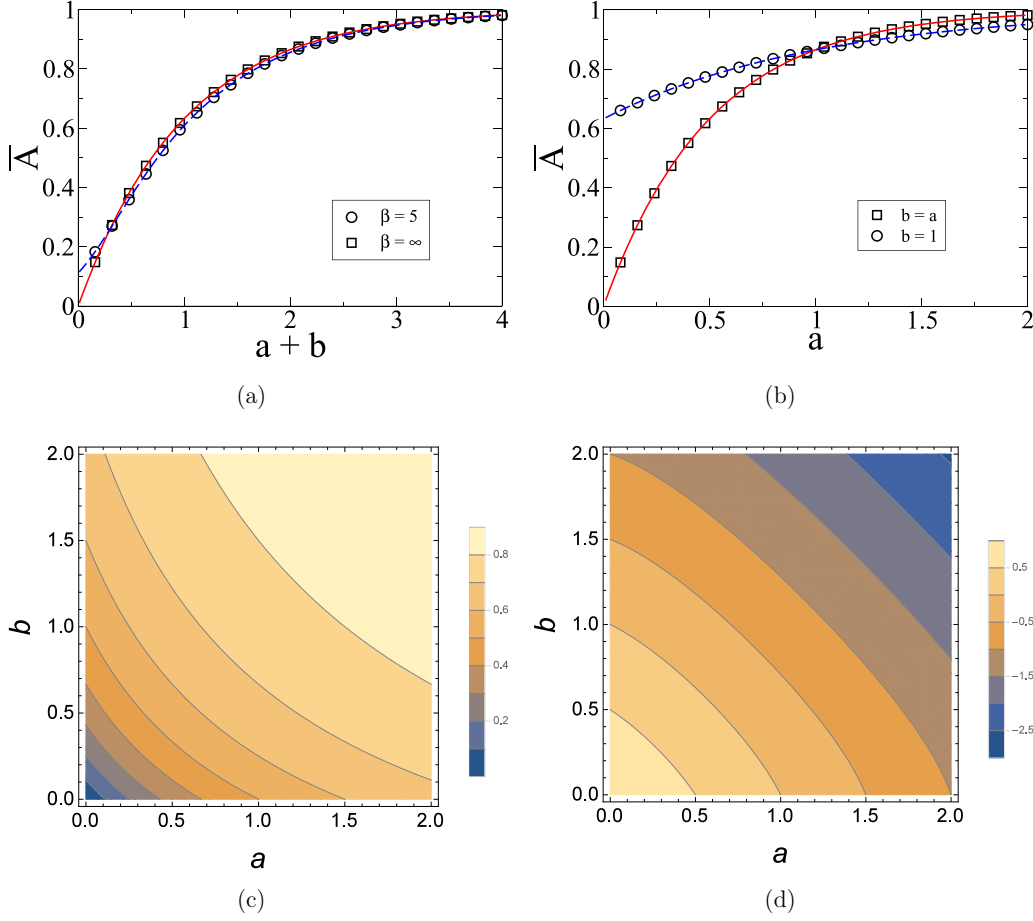


FIG. 2. The mean connectivity of the optimized directed network in Model A with exponentially distributed (nonnegative) edge weights. (a) Both the outward and inward node weights are homogeneous, with the respective node strength characterized by a and b . Metropolis Monte Carlo simulation of the average mean connectivity at finite temperature with $\beta = 5$ is shown by the \circ symbols. The fully optimized (zero-temperature) mean connectivity measured in simulations, performed with the algorithm in Sec. VI, is denoted by the \square symbols. The corresponding theoretical results are denoted by the solid and dashed curves. (b) Both the inward and outward node weight distributions are exponential decay functions. The fully optimized (zero-temperature) mean connectivity measured plotted as a function of a in simulations for exponentially distributed (nonnegative) inward and outward node weights. The corresponding theoretical result is denoted by the solid ($b = a$) and dashed ($b = 1$) curves. (c) Contour plot of the mean connectivity of the optimized network in panel (b) as a function of a and b . (d) Contour plot of the cost of the optimized network as a function of a and b for the case in panel (c).

diagram” shown in Fig. 3(a):

$$\begin{aligned} \bar{A}_4 = 0, \quad \bar{A}_3 = \frac{(a+b-1)^2}{2ab}, \quad \bar{A}_2 = 1 - \frac{1}{2ab}, \\ \bar{A}_1 = 1 + \frac{a}{2b} - \frac{1}{b}, \quad \bar{A}_{1'} = 1 + \frac{b}{2a} - \frac{1}{a}. \end{aligned} \quad (24)$$

Here the subscript of \bar{A} denotes the corresponding region in Fig. 3(a). To verify the above analytic formula, simulations are performed along the $b = a$ line for different values of a whose mean connectivity are measured and shown in Fig. 3(b). The corresponding theoretical result can be obtained from Eq. (24) to give

$$\bar{A} = \begin{cases} 0 & a \leq \frac{1}{2}, \\ \frac{(2a-1)^2}{2a^2} & \frac{1}{2} < a \leq 1, \\ 1 - \frac{1}{2a^2} & 1 < a, \end{cases} \quad (25)$$

which also is plotted in Fig. 3(b) showing perfect agreement. Simulations for fixed $b = 2$ for different values of a are also carried out [see Fig. 3(b) also], with the theoretical result derived to be

$$\bar{A} = \begin{cases} 0 & a \leq -2, \\ \frac{1}{2} + \frac{a}{4} & -2 < a \leq 1, \\ 1 - \frac{1}{4a} & 1 < a, \end{cases} \quad (26)$$

again showing perfect agreement [dashed curve in Fig. 3(b)].

IV. MODEL B: MEAN-FIELD EQUATIONS AND PHASE TRANSITIONS

To model the cooperative effect of the formation of an edge that is enhanced by the existence of another edge, one can model such interactions on a “mean-field” level by the

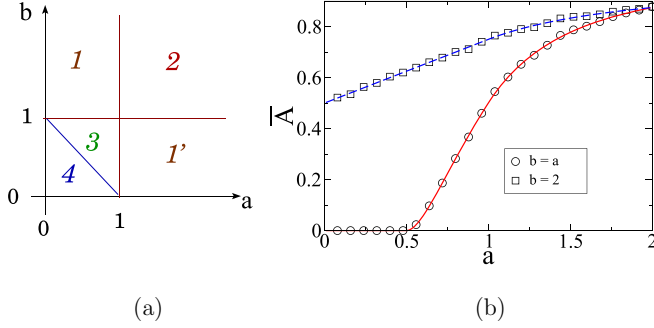


FIG. 3. Optimized network in Model A with uniform distribution of node weights in some finite domain, $p_{\text{in}}(r) = 1$ and $p_{\text{out}} = 1$ for $r, s \in [0, 1]$ and $= 0$ otherwise. The edges are unweighted with $p(w) = \delta(w - 1)$. (a) b vs a phase diagram showing regions with different expression for the optimized mean connectivity as given by Eq. (24). (b) Simulation results for the optimized mean connectivity \bar{A} as a function of a for the cases of $b = a$ and $b = 2$. The corresponding theoretical results are denoted by the solid and dashed curves.

following cost function, which we called Model B, as

$$\begin{aligned} C_B &= \sum_{i \neq j} w_{ij} A_{ij} - \frac{1}{N_b} \left(\sum_{i=1}^N \lambda_i^{\text{in}} k_i^{\text{in}} + \sum_{i=1}^N \lambda_i^{\text{out}} k_i^{\text{out}} \right)^2 \\ &= \sum_{\gamma} w_{\gamma} A_{\gamma} - \frac{1}{N_b} \left(\sum_{\gamma=1}^{N_b} \Lambda_{\gamma} A_{\gamma} \right)^2, \end{aligned} \quad (27)$$

where Λ_{α} is also given by Eq. (3). The two terms in C_B have similar physical meaning as that of Model A given by Eq. (2). The main difference is that the tendency to make connections in Model A increases linearly with the weighted sum of the local degree, whereas in Eq. (27) such a tendency to make connection is quadratic so as to model the simplest cooperative or nonlinear effects in forming the connections, which in turn can lead to more interesting phase transitions. Again with the Ising spin defined as $S_{\gamma} = 2A_{\gamma} - 1$, one obtains the Hamiltonian of Ising spin system

$$\mathcal{H}_B = -\frac{1}{2} \sum_{\gamma} (\bar{\Lambda} \Lambda_{\gamma} - w_{\gamma}) S_{\gamma} - \frac{1}{4N_b} \left(\sum_{\gamma} \Lambda_{\gamma} S_{\gamma} \right)^2, \quad (28)$$

which consists of an external field term and an interaction term (second term) with $\Lambda_{\gamma} \Lambda_{\gamma'}$ being the strength of interactions between two spins S_{γ} and $S_{\gamma'}$. The statistical mechanics of this model can be solved by performing the Hubbard-Stratonovich transformation to calculate the partition function to give

$$\begin{aligned} Z &= \sqrt{\frac{\beta N_b}{4\pi}} \int_{-\infty}^{\infty} \exp \left\{ -\frac{\beta N_b}{4} y^2 \right. \\ &\quad \left. + \sum \ln 2 \cosh \frac{\beta}{2} \left[(\bar{\Lambda} + y) \Lambda_{\gamma} - w_{\gamma} \right] \right\} dy, \end{aligned} \quad (29)$$

which leads to the saddle-point equation in the large N_b limit given by

$$\begin{aligned} y_o &= \frac{1}{N_b} \sum_{\gamma} \Lambda_{\gamma} \tanh \left\{ \frac{\beta}{2} [(\bar{\Lambda} + y_o) \Lambda_{\gamma} - w_{\gamma}] \right\} \\ &\rightarrow \int d\Lambda \int dw P(\Lambda, w) \Lambda \tanh \left\{ \frac{\beta}{2} [(\bar{\Lambda} + y_o) \Lambda - w] \right\}. \end{aligned} \quad (30)$$

$$\rightarrow \int d\Lambda \int dw P(\Lambda, w) \Lambda \tanh \left\{ \frac{\beta}{2} [(\bar{\Lambda} + y_o) \Lambda - w] \right\}. \quad (31)$$

y_o represents the modified order-parameter (or weighted magnetization), $y_o \equiv \frac{1}{N_b} \sum_{\gamma} \Lambda_{\gamma} S_{\gamma}$. For the fully optimized solution for the network model, the ground state should be considered (i.e., $\beta \rightarrow \infty$). Here, we introduce a new parameter u_o defined as $u_o \equiv \frac{1}{N_b} \sum_{\gamma} \Lambda_{\gamma} A_{\gamma} \equiv \bar{\Lambda} \bar{A}$. Assuming $P(\Lambda, w) = \mathbf{P}(\Lambda)P(w)$, we derive the saddle-point equation governing the connectivity of the fully optimized (zero-temperature) network:

$$u_o = \iint d\lambda_1 d\lambda_2 P_{\text{out}}(\lambda_1) P_{\text{in}}(\lambda_2) (\lambda_1 + \lambda_2) F_w[2u_o(\lambda_1 + \lambda_2)]. \quad (32)$$

The mean connectivity of the optimized network is given by

$$\bar{A} = \iint d\lambda_1 d\lambda_2 P_{\text{out}}(\lambda_1) P_{\text{in}}(\lambda_2) F_w[2u_o(\lambda_1 + \lambda_2)], \quad (33)$$

where u_o is obtained from the root of Eq. (32). It is clear that $u_o = 0$ (corresponds to network with no edge at all) is always the trivial root for nonnegative edge weights.

A. Mean-field equations for Model B

In addition to the saddle-point equation for u_o which describes the mean properties of the whole system, one can employ the mean-field theory to derive the local mean-field equations for the local magnetizations or network connections. To carry out the mean-field approximation, the spin in Eq. (28) is replaced by its mean value $m_{\gamma} \equiv \langle S_{\gamma} \rangle$, and the Hamiltonian becomes

$$\begin{aligned} \mathcal{H}_B &= -\frac{1}{2} \sum_{\gamma} (\bar{\Lambda} \Lambda_{\gamma} - w_{\gamma}) S_{\gamma} \\ &\quad - \frac{1}{4N_b} \sum_{\gamma} \sum_{\gamma'} \Lambda_{\gamma'} \Lambda_{\gamma} (m_{\gamma'} + \delta s_{\gamma'}) (m_{\gamma} + \delta s_{\gamma}), \end{aligned} \quad (34)$$

where δs_{γ} is the fluctuation from the mean value, $S_{\gamma} = m_{\gamma} + \delta s_{\gamma}$. Ignoring spin fluctuations of $\mathcal{O}(\delta s^2)$ and higher, we obtain the Hamiltonian under the mean-field approximation:

$$\begin{aligned} \mathcal{H}_B^{\text{MF}} &= -\frac{1}{2} \sum_{\gamma} \left[\left(\bar{\Lambda} + \frac{1}{N_b} \sum_{\gamma'} \Lambda_{\gamma'} m_{\gamma'} \right) \Lambda_{\gamma} - w_{\gamma} \right] \\ &\quad \times S_{\gamma} - \frac{1}{4N_b} \left(\sum_{\gamma} \Lambda_{\gamma} m_{\gamma} \right)^2. \end{aligned} \quad (35)$$

Now, the mean-field Hamiltonian of Model B share the same form as in Model A and one can obtain the local mean-field equations

$$\begin{aligned} m_{\gamma} &= \tanh \frac{\beta}{2} \left[\left(\bar{\Lambda} + \frac{1}{N_b} \sum_{\gamma'} \Lambda_{\gamma'} m_{\gamma'} \right) \Lambda_{\gamma} - w_{\gamma} \right], \\ &\times \gamma = 1, 2, \dots, N_b, \end{aligned} \quad (36)$$

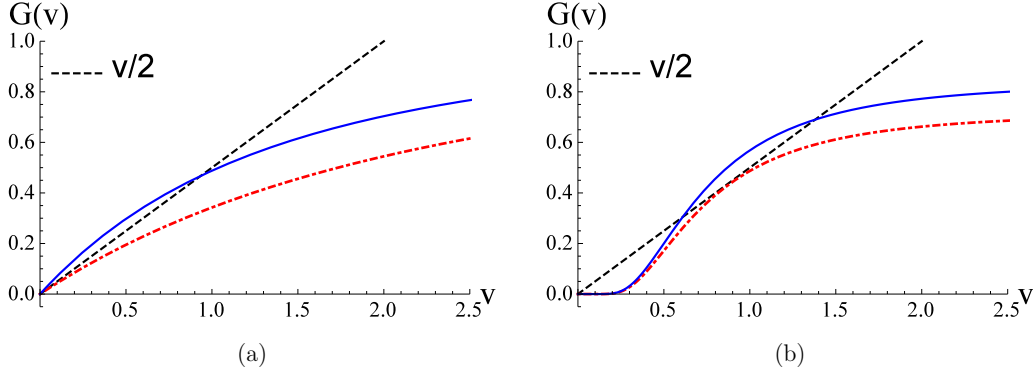


FIG. 4. (a) The general scenario of $G''_{a,b}(v) < 0$ holds, exhibiting a second-order transition. For $G'_{a,b}(0) < \frac{1}{2}$ (red dot-dashed curve), only the trivial $v = 0$ root for the saddle-point Eq. (39) which corresponds to situation that the optimized solution is an unconnected network. For $G'_{a,b}(0) > \frac{1}{2}$ (blue solid curve), another nontrivial $v > 0$ root exists corresponding to a network with finite connections. (b) The scenario that $G_{a,b}(v)$ has an inflexion point, i.e., $G''_{a,b}(v) = 0$ at some $v > 0$, a first-order phase transition is possible. As the parameters (a, b) vary to (a^*, b^*) , a nontrivial root emerge via a tangent bifurcation at $v = v^*$ (the red dot-dashed curve). Further change in the parameters result in two nontrivial roots v_1 and v_2 as shown by the blue solid curve.

which is consistent with the saddle-point equation for y_o in Eq. (30). The local mean-field equations can also be derived using the cavity method in interacting Ising spin systems (see the review [16]). In addition, it is worth to note that in general the correct equation for local magnetization for heterogeneous coupling strengths (especially with ferro and antiferro couplings) is the Thouless-Anderson-Palmer (TAP) equation [19]. However, due to the $1/N_b$ factor in the spin-spin coupling term of the Hamiltonian (28), the TAP equation reduces to Eq. (36) in the thermodynamic limit ($N_b \rightarrow \infty$) since the reaction term in the TAP equation is of order N_b times smaller than the mean-field term.

In the zero-temperature limit with $m_\gamma = 2A_\gamma - 1$, one can derive the mean-field equations for the optimized directed link configurations from Eq. (36):

$$A_\gamma = \Theta(2\overline{\Lambda A} \Lambda_\gamma - w_\gamma), \quad \gamma = 1, 2, \dots, N_b, \quad (37)$$

which are coupled nonlinear equations for the A_γ 's.

B. Classification of phase transitions in Model B

Hereafter, we shall focus on edge and node weight distributions as given by Eqs. (13) and (14). Introducing the scaled variable $v \equiv 2u_o/w_o = \frac{2}{w_o} \overline{\Lambda A}$, the mean-field equations (37) can be rewritten as

$$A_\alpha = \Theta(v w_o \Lambda_\alpha - w_\alpha), \quad \alpha = 1, 2, \dots, N_b, \quad (38)$$

and v satisfies the saddle-point equation

$$\begin{aligned} \frac{v}{2} &= \iint dr ds p_{\text{in}}(r) p_{\text{out}}(s) (as + br) f_w(v[as + br]) \\ &\equiv G_{a,b}(v), \end{aligned} \quad (39)$$

where $a \equiv \frac{\lambda_o^{\text{out}}}{\sqrt{w_o}}$ and $b \equiv \frac{\lambda_o^{\text{in}}}{\sqrt{w_o}}$ for Model B. The mean connectivity and optimized cost can be directly calculated to give

$$\bar{A} = \iint dr ds p_{\text{in}}(r) p_{\text{out}}(s) f_w(v[as + br]), \quad (40)$$

$$\frac{C_B}{N_b w_o} = \iint dr ds p_{\text{in}}(r) p_{\text{out}}(s) \int^{(as+br)v} dz z p(z) - \frac{v^2}{4}, \quad (41)$$

where v is the root of the saddle-point equation (39). In general, $G_{a,b}(v) \leq \iint dr ds p_{\text{in}}(r) p_{\text{out}}(s) (as + br)$ and hence is bounded. Since w is nonnegative, $G'_{a,b}(v) = \iint dr ds p_{\text{in}}(r) p_{\text{out}}(s) (as + br)^2 p(v[as + br]) \geq 0$, i.e., $G_{a,b}(v)$ is a nondecreasing function in v . There can be two general and one special scenarios determining the nature of the phase transitions.

The first general scenario is that $G''_{a,b}(v) < 0$ always holds, which will lead to a second-order phase transition as explained below. Since $G_{a,b}(v)$ is nondecreasing and bounded by its value at large v [see Fig. 4(a) for a schematic illustration], Eq. (39) implies a nontrivial root of the saddle-point equation emerges for $G'_{a,b}(0) > \frac{1}{2}$. And if the associated cost $C_B < 0$, which will be further demonstrated below, then a continuous second-order phase transition results. The second-order transition occurs at (a_c, b_c) and the phase boundary can be derived from $G'_{a_c, b_c}(0) = \frac{1}{2}$ to be

$$2p(0)I_2 = 1, \quad I_n \equiv \iint dr ds p_{\text{in}}(r) p_{\text{out}}(s) (a_c s + b_c r)^n. \quad (42)$$

Remarkably, the critical phase boundary curve depends on $p(0)$ but does not depend on the detail shape of the edge weight distribution. The properties of the continuous transition can be further investigated by examining the behavior near (a_c, b_c) in the $v \gtrsim 0$ (ordered or finite-connectivity) phase by expanding the solution of v in Eq. (39) in powers of the deviation from criticality, i.e., in powers of $G'_{a,b}(0) - \frac{1}{2}$. For $p'(0) \neq 0$, using $G''_{a,b}(0) = p'(0)I_3$, direct calculations give

$$v \simeq \frac{2(G'_{a,b}(0) - \frac{1}{2})}{-p'(0)I_3} + \mathcal{O}\left\{\left[G'_{a,b}(0) - \frac{1}{2}\right]^2\right\}, \quad (43)$$

and the mean connectivity near the phase boundary in the finite-connectivity phase is

$$\bar{A} \simeq \frac{2p(0)I_1}{-p'(0)I_3} \left[G'_{a,b}(0) - \frac{1}{2}\right] + \mathcal{O}\left\{\left[G'_{a,b}(0) - \frac{1}{2}\right]^2\right\}, \quad (44)$$

with a critical exponent of unity. Furthermore, the optimized cost in Eq. (41) for the nontrivial solution can be expanded to

$\mathcal{O}(v^3)$ to give

$$\frac{C_B}{w_o N_b} \simeq -\frac{2[G'_{a,b}(0) - \frac{1}{2}]^3}{3[p'(0)I_3]^2} + \mathcal{O}\left\{\left[G'_{a,b}(0) - \frac{1}{2}\right]^4\right\}, \quad (45)$$

which is always negative in the finite-connectivity phase and hence is the optimized network. If $p'(0) = 0$ and the lowest order nonvanishing derivative is n (i.e., $p^{(n)} \neq 0$), similar calculations can also be carried out. For instance, $\bar{A} \sim [G'_{a,b}(0) - \frac{1}{2}]^{\frac{1}{n}}$, i.e., the critical exponent is $\frac{1}{n}$.

The second general scenario is that $G_{a,b}(v)$ has an inflexion point, i.e., $G''_{a,b}$ changes sign, and a first-order transition can occur. In this case, a nontrivial root emerges via a tangent (saddle-node) bifurcation that occurs at (a^*, b^*) with $v = v^*$ [see the schematic illustration in Fig. 4(b)]. Further changes in (a, b) results in a pair of nontrivial roots (denoted by v_1 and v_2) as illustrated by the blue solid curve in Fig. 4(b). The abrupt occurrence of nontrivial and noninfinitesimal $v > 0$ roots for infinitesimal changes of (a, b) beyond (a^*, b^*) leads to a first-order transition. v^* satisfies Eq. (39) together with

$$G'_{a^*,b^*}(v^*) = \frac{1}{2}. \quad (46)$$

However, in many scenarios the corresponding cost C_B for the nontrivial root(s) may still be positive and the zero-cost unconnected network is still the optimized one. As the parameters a and b are varied, C_B for the nontrivial root can become negative and a first-order transition occurs. In this case, a first-order transition occurs at $v = v_t$ and the phase boundary can be determined from the conditions:

$$C_B(v_t) = 0, \quad G_{a,b}(v_t) = \frac{v_t}{2}. \quad (47)$$

In general, one needs to examine the corresponding costs of the nontrivial roots emerged [say v_1 and v_2 as shown in

$$\frac{v}{2} = G_{a,b}(v) = \frac{be^{-\frac{1}{bv}}(bv+1) - ae^{-\frac{1}{av}}(av+1)}{v(b-a)} \xrightarrow{b \rightarrow a} \frac{[1+2av(1+av)]e^{-\frac{1}{av}}}{av^2}, \quad (48)$$

$$\bar{A} = \frac{be^{-\frac{1}{bv}} - ae^{-\frac{1}{av}}}{(b-a)} \xrightarrow{b \rightarrow a} \frac{(1+av)e^{-\frac{1}{av}}}{av}, \quad (49)$$

$$\frac{C_B}{N_b w_o} = \bar{A} - \frac{v^2}{4} = \frac{be^{-\frac{1}{bv}} - ae^{-\frac{1}{av}}}{(b-a)} - \frac{v^2}{4}. \quad (50)$$

From Eq. (48), one gets $G''_{a,b}(v) = \frac{(a-3abv)e^{-\frac{1}{bv}} - (b-3abv)e^{-\frac{1}{av}}}{ab(b-a)v^5}$ and hence there is an inflexion point at some finite $v > 0$, and thus nontrivial root v^* emerges via tangent bifurcation given by Eq. (48) and $\frac{1}{2} = G'_{a,b}(v^*) = \frac{e^{-\frac{1}{bv^*}} - e^{-\frac{1}{av^*}}}{(b-a)v^{*3}}$. In addition, the tangent bifurcation boundary curve for the emergence of nontrivial root, $\phi_{\text{bif}}(a, b) = 0$, can be obtained by eliminating v in Eq. (48) and $G'_{a,b}(v) = \frac{1}{2}$ which reads

$$\frac{e^{-\frac{1}{bv}} - e^{-\frac{1}{av}}}{(b-a)v^3} = \frac{be^{-\frac{1}{bv}}(bv+1) - ae^{-\frac{1}{av}}(av+1)}{v^2(b-a)} = \frac{1}{2}. \quad (51)$$

$\phi_{\text{bif}}(a, b) = 0$ is shown by the dashed curve in Fig. 5(a). Careful examination reveals that the cost of the emerged nontrivial root $C_B(v^*)$ is positive and hence the unconnected network is still the optimized solution. Upon further changes in the

Fig. 4(b)], and together with the zero-cost of the trivial unconnected solution, the optimized solution is given by the one with the lowest cost. And a first-order transition occurs when there is a switch in the lowest cost among $C_B(0) = 0$, $C_B(v_1)$, and $C_B(v_2)$.

Finally, in some special cases, it is possible that the root v^* emerges at the tangent bifurcation has a cost $C_B(v^*) \leq 0$, then a hybrid phase transition results [13]. Such hybrid phase transition exhibits characteristics of a first-order (a jump in the mean connectivity) and second-order [a continuous power-law increase of mean-connectivity for small variations of the parameters beyond (a^*, b^*)] phase transitions. As the parameters vary beyond the hybrid phase transition boundary, the optimized solution is given by v_i ($i = 1$ or 2) where $C_B(v_i) = \min[C_B(v_1), C_B(v_2)]$.

C. Equal edge weight distribution: $P(w) = \delta(w - w_o)$

In this case $f_w(w) = \Theta(w - 1)$, it is easy to see from Eq. (39) that $G'_{a,b}(0) = 0$. Here we consider nonnegative node weights, i.e. $p_{\text{in}}(r), p_{\text{out}}(s)$ with $r, s \in [0, \infty)$, hence $G_{a,b}(v \rightarrow \infty) \rightarrow$ a positive constant. Since $G_{a,b}(v)$ is not a constant and nondecreasing, thus there must be an inflexion point ($G''_{a,b} = 0$) at some finite value of v which is the scenario as depicted in Fig. 4(b). Therefore, for the case of unweighted edge, there is in general a first-order phase transition, which will be demonstrated explicitly below.

Here we take the node weights to follow exponential decay distributions with nonnegative weights, i.e., $p_{\text{in}}(r) = e^{-r}$, $p_{\text{out}}(s) = e^{-s}$ where $r, s, \in [0, \infty)$. Using Eqs. (39)–(41), after some algebra, one obtains (recall $a \equiv \frac{\lambda_o^{\text{out}}}{\sqrt{w_o}} > 0$ and $b \equiv \frac{\lambda_o^{\text{in}}}{\sqrt{w_o}} > 0$)

parameters away from the bifurcation boundary, the cost of one of the nontrivial root (the larger one) decreases and becomes negative at some threshold signifying a first-order phase transition, whose conditions are given by Eq. (47), which in this case reads

$$\frac{v}{2} = \sqrt{\frac{be^{-\frac{1}{bv}} - ae^{-\frac{1}{av}}}{(b-a)}} = \frac{be^{-\frac{1}{bv}}(bv+1) - ae^{-\frac{1}{av}}(av+1)}{v(b-a)}, \quad (52)$$

and the solution gives the first-order boundary curve as shown in Fig. 5(a).

The above theoretical results are further verified by simulations for the measured mean connectivity as displayed in Fig. 5(b) showing perfect agreement with the analytic formula. For case of $b = a$, in this case a^* for the tangent

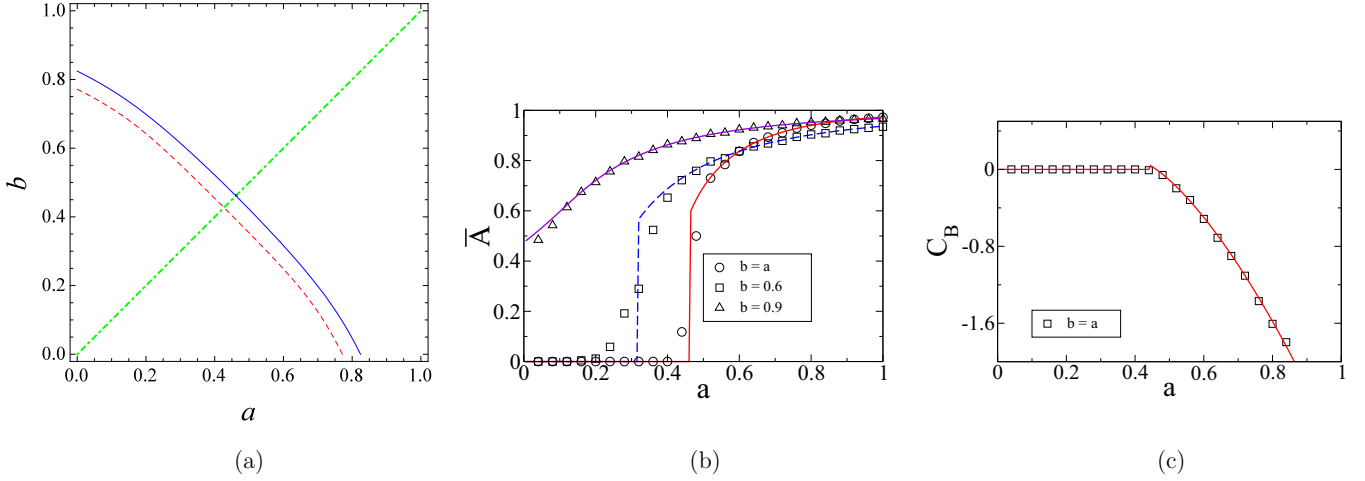


FIG. 5. Optimized directed network in Model B with edges of equal weights and nonnegative exponentially distributed inward and outward node weights. (a) Phase diagram showing the boundary (the red dashed curve) separating the emergence of nontrivial roots via tangent bifurcation, $\phi_{bif}(a, b) = 0$. The boundary curve for zero optimized cost, $C_B = 0$, which is also the first-order phase boundary is shown by the solid blue curve. (b) Simulation results of the optimized network for \bar{A} vs a the cases of $b = 0.9$ and $b = 0.6$. The respective theoretical predictions from Eqs. (48) and (49) for \bar{A} are also shown. (c) The (normalized) cost, $\frac{C_B}{N_b w_o}$, of the optimized network measured in simulations (symbols) as a function of a for the case of $b = a$. The lowest cost among the costs of all roots of the saddle-point equation (48) is shown by the solid curve. The cost is zero for the trivial no connection network, the (lower cost) nontrivial solution emerged at $a^* \simeq 0.4270$ also has a positive cost, and its cost decreases with a and becomes negative for $a > a_t = \frac{e^{\frac{1}{\sqrt{2}}}}{2\sqrt{2(1+\sqrt{2})}} \simeq 0.46149$. a^* and a_t are marked by vertical dotted lines.

bifurcation point and a_t for the first-order transition point can be derived analytically to be

$$a^* = \frac{s^{*2} e^{\frac{1}{2s^*}}}{\sqrt{2}}, \text{ where}$$

$$s^* = \frac{3}{1 + \sqrt[3]{37 - 3\sqrt{114}} + \sqrt[3]{37 + 3\sqrt{114}}} \simeq 0.44062 \quad (53)$$

$$\text{is the real root of } 2s^{*3} + 2s^{*2} + s^* = 1, \quad (54)$$

$$a_t = \frac{e^{\frac{1}{\sqrt{2}}}}{2\sqrt{2(1+\sqrt{2})}} \simeq 0.46149. \quad (55)$$

The simulation results indicate a sharp jump in \bar{A} near $a = 0.46$ in close agreement with the theoretical a_t . The simulations are performed with a single realization of the edge and node distribution and strong realization fluctuations are observed near the transition in the simulations, average over many realizations will render the simulation results in even better agreement with the theoretical results, as observed in previous studies on undirected optimized networks [13]. The simulation result of the optimized cost is also displayed as a function of a for $b = a$ in Fig. 5(c). The theoretical cost as given by Eq. (50) is also shown (solid curve). Notice that the cost is zero for the trivial no connection network, the (lower cost) nontrivial solution emerged at $a^* \simeq 0.4270$ also has a positive cost, and its cost decreases with a and becomes negative for $a > a_t \simeq 0.46149$.

D. Model B with homogeneous node weights: First- and second-order phase transitions

In this case, the nodes have the same inward weights and the same outward weights with $p_{in}(r) = \delta(r - 1)$ and $p_{out}(s) = \delta(s - 1)$. The optimized mean connectivity and cost can be directly obtained from Eqs. (40) and (41) to be

$$\bar{A} = f_w[(a+b)v_r],$$

$$\times \frac{C_B}{N_b w_o} = \int^{(a+b)v_r} dz z p(z) - (a+b)^2 \bar{A}^2, \quad (56)$$

where v_r is the lowest-cost root of the saddle-point equation (39),

$$v/2 = G_{a,b}(v) \equiv (a+b)f_w[(a+b)v], \text{ and}$$

$$G'_{a,b}(v) = (a+b)^2 p[(a+b)v]. \quad (57)$$

The behavior of the network is determined by the single parameter $a+b$. The increase of either a (outward node weight) or b (inward node weight) will enhance the network connections of the network.

Depending on the properties of the edge distribution f_w , the optimized directed network can exhibit a variety of different phase transitions as described in the previous section, which will be illustrated below. First consider the edge distribution of the form

$$p(w) = \frac{w^\alpha e^{-w}}{\Gamma(1+\alpha)}, \quad w \in [0, \infty); \quad \alpha \geq 0, \quad (58)$$

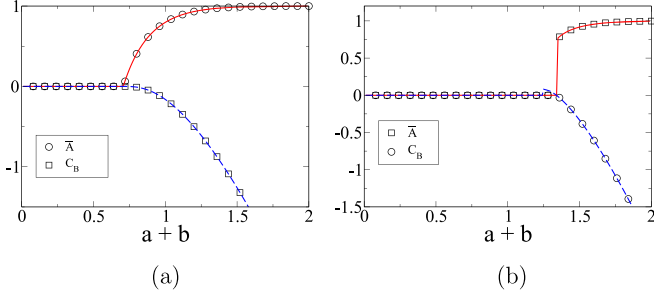


FIG. 6. (a) Second-order transition of the directed Model B with unweighted nodes and exponential edge weight distribution given by Eq. (58) with $\alpha = 0$. The optimized mean-connectivity as a function of $a + b$ (dashed curve). The optimized cost as a function of $a + b$ (solid curve). The simulation results (symbols) are also plotted. (b) First-order transition of the directed Model B with unweighted nodes and edge weight distribution given by Eq. (58) with $\alpha = 1$. Simulation results (symbols) for the optimized mean-connectivity as a function of $a + b$ showing a transition close to the theoretical value of $(a + b)_t \simeq 1.34$ (marked by vertical dotted line). The solid curve is the theoretical result as given by Eq. (62). Simulation results (symbols) of the normalized cost of the network as a function of $a + b$. The cost as given by Eq. (60) (blue dashed curve) is zero for the trivial no connection network, the (lower cost) nontrivial solution emerged at $(a + b)^* \simeq 1.23$ also has a positive cost, and its cost decreases becomes negative for $a + b > (a + b)_t \simeq 1.34$. $(a + b)^*$ and $(a + b)_t$ are marked by vertical dotted lines.

and the cumulative distribution is given by $f_w(z) = 1 - \frac{\Gamma_{1+\alpha}(z)}{\Gamma(1+\alpha)}$. Other relevant quantities can be directly obtained from Eqs. (56) and (57):

$$G_{a,b}(v) = (a + b) \left[1 - \frac{\Gamma_{1+\alpha}((a + b)v)}{\Gamma(1 + \alpha)} \right],$$

$$G'_{a,b}(v) = \frac{(a + b)^{2+\alpha}}{\Gamma(1 + \alpha)} v^\alpha e^{-(a+b)v}, \quad (59)$$

$$\bar{A} = 1 - \frac{\Gamma_{1+\alpha}((a + b)v_r)}{\Gamma(1 + \alpha)},$$

$$\frac{C_B}{N_b w_o} = 1 + \alpha - \frac{\Gamma_{2+\alpha}((a + b)v_r)}{\Gamma(1 + \alpha)} - (a + b)^2 \bar{A}^2. \quad (60)$$

For $\alpha = 0$ and hence $p(z)$ is monotonic decreasing, the optimized network exhibits a second-order phase transition to be shown as follows. In this case, $f_w(z) = 1 - e^{-z}$ and the saddle-point equation reads $v/2 = G_{a,b}(v) = (a + b)[1 - e^{-(a+b)v}]$. Thus, $G''_{a,b}(v)$ is always negative and thus a second-order transition is given by $G'_{a,b}(0) = \frac{1}{2}$ [see Fig. 4(a)] and occurs at $a + b = \frac{1}{\sqrt{2}}$. The mean connectivity given by Eq. (60) can be directly calculated to give $\bar{A} = [1 - e^{-(a+b)v_r}] \Theta(a + b - \frac{1}{\sqrt{2}})$ where v_r is the nontrivial root given by the saddle-point equation $v_r/2 = (a + b)[1 - e^{-(a+b)v_r}]$. In addition, it can be verified that $C_B(v_r)$ is always negative justifying that the nontrivial root has a lower cost. Simulations are performed and the measured results for \bar{A} as a function of $a + b$ are plotted in Fig. 6(a) together with the above theoretical result showing perfect agreement.

For the case of $\alpha > 0$, $p(w)$ exhibits a peak and $G_{a,b}(v)$ has an inflexion point [see Fig. 4(b)], the optimized network has

a first-order transition to be described below. Take $\alpha = 1$ for example, then $G_{a,b}(v) = (a + b)(1 - [1 + (a + b)v]e^{-(a+b)v})$ and direct calculations indicates that the nontrivial root v^* of the saddle-point equation emerges at $(a + b)^*$ via tangent bifurcation, which can solved from Eq. (57) to be $(a + b)^* = \sqrt{\frac{e^{z^*}}{2z^*}} = 1.2944$ where $z^* = 1.7933$ is the nonzero root of $e^z = z^2 + z + 1$; and $v^* = \frac{e^{z^*}}{2} = 1.3854$. But the corresponding cost $C_B(v^*)$ still remains positive and thus not the optimized solution. Upon further increasing $a + b$, there are two nontrivial roots and the cost of the larger root (v_2) decreases and its cost becomes zero at the first-order transition point $a + b = (a + b)_t$ with $v_2 = v_t$. $(a + b)_t$ and v_t can be obtained by solving Eq. (47) and $C_B = 0$ with $G_{a,b}$ and C_B given by Eqs. (59) and (60). After some algebra, one gets the first-order transition threshold

$$(a + b)_t = \sqrt{\frac{y_t}{2[1 - (1 + y_t)e^{-y_t}]}} = 1.33941,$$

where $y_t = 2.688$, (61)

which is the nonzero root of $4 - y = e^{-y}(4 + 3y + y^2)$ (62)

and $v_t = \sqrt{2y_t[1 - (1 + y_t)e^{-y_t}]} = 2.0069$. (63)

Figure 6(b) plots the simulation results of measured mean connectivity of the optimized network \bar{A} as a function of $a + b$ with $\alpha = 1$ showing an abrupt jump signifying the first-order transition at $(a + b)_t \approx 1.34$ in close agreement with the theoretical value.

The diversity in phase transitions of the model can be illustrated by the edge distributions of the form

$$p(w) = \frac{(w + \alpha)e^{-w}}{1 + \alpha}, \quad w \in [0, \infty); \quad \alpha \geq 0. \quad (64)$$

The cumulative distribution is given by $f_w(z) = 1 - (1 + \frac{z}{1+\alpha})e^{-z}$. Other relevant quantities can be directly calculated similarly using Eqs. (56) and (57). The diverse phase transitions can be demonstrated in the phase diagram of α versus $a + b$ displayed in Fig. 7(a), showing both first- and second-order phase boundaries which are obtained analytically. Critical phase transition occurs for $\alpha > 1$ whose phase boundary can be derived from $G'_{a,b}(0) = \frac{1}{2}$ using Eq. (59) to give $(a + b)_c = \sqrt{\frac{1+\alpha}{2\alpha}}$. First-order transition takes place for $\alpha < 1$ whose phase boundary can be derived from Eq. (47). The first- and second-order phase boundary merged at the critical point of $\alpha = 1$ and $a + b = 1$. The change in the nature of the phase transitions at $\alpha = 1$ can be attributed to the form of the edge distribution in Eq. (64) that $p(w)$ is monotonic decreasing for $\alpha > 1$ but exhibits a peak for $\alpha < 1$ (thus, $G_{a,b}$ has an inflexion point and hence the first-order transition). Simulations are performed to measure the mean-connectivity of the optimized networks as a function of $a + b$ for different values of α as plotted in Fig. 7(b) showing the characteristics of first- and second-order transitions for $\alpha < 1$ and $\alpha > 1$, respectively. The theoretical values obtained from Eq. (56) are also plotted showing perfect agreement with the simulation results.

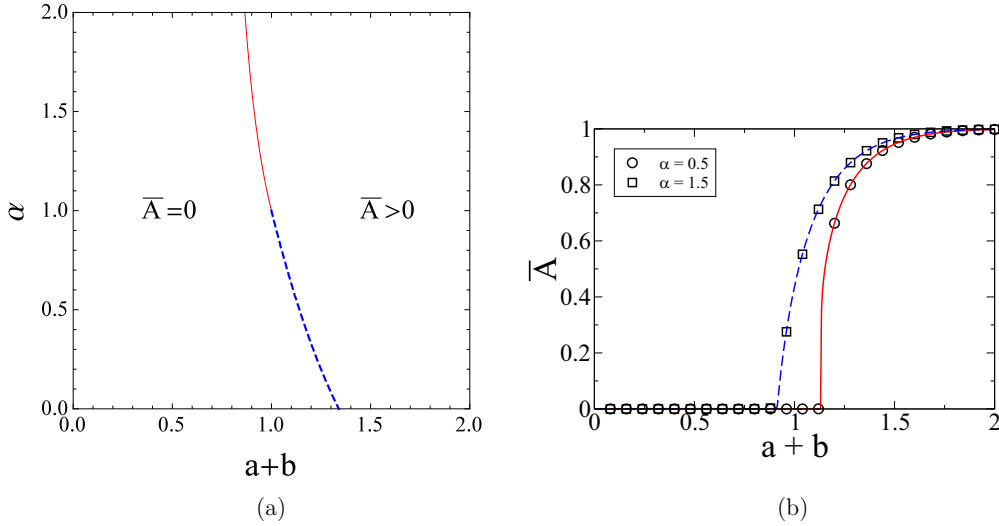


FIG. 7. First- and second-order phase transitions in the directed Model B with unweighted nodes and edge weight distribution given by Eq. (64). (a) Phase diagram of α vs $a + b$. The first- and second-order phase boundaries are denoted by the blue dashed and red solid curves, respectively. The first- and second-order phase boundary meets at the tricritical point of $\alpha = 1$ and $a + b = 1$. (b) Simulation results for the optimized mean-connectivity as a function of $a + b$ showing a first-order transition for $\alpha = 0.5$ and a second-order transition for $\alpha = 1.5$. The simulation results (symbols) indicate a sharp jump in \bar{A} at $a + b = (a + b)_t \simeq 1.1413$ for $\alpha = 0.5$ which is very close to the bifurcation point for nontrivial root at $(a + b)^* \simeq 1.13404$. The theoretical result (blue dashed curve) is also shown. For for $\alpha = 1.5$, a second-order phase transition occurs at $(a + b)_c = \sqrt{\frac{1+\alpha}{2\alpha}} = 0.91287$. The theoretical result (red solid curve) is also shown.

E. General phase diagrams in Model B

Here we consider some general, common but nontrivial node and edge weight distributions. The key formulas for general analytic calculations have been listed in Eqs. (39)–(41). In general, the phase diagram of b versus a with the corresponding phase boundaries can be obtained analytically. For illustration, consider the case of exponential decay distributions for all nonnegative node and edge weights, namely: $p_{\text{in}}(r) = e^{-r}$, $p_{\text{out}}(s) = e^{-s}$, $p(w) = e^{-w}$, where $r, s, w \in [0, \infty)$. From Eqs. (39)–(41), after some algebra, one can derive

$$G_{a,b}(v) = a + b + \frac{a^2}{(b-a)(1+av)^2} - \frac{b^2}{(b-a)(1+bv)^2} \xrightarrow{b \rightarrow a} 2a \left(1 - \frac{1}{(1+av)^3} \right), \quad (65)$$

$$\bar{A} = \frac{(a+b+abv)v}{(1+av)(1+bv)}, \quad (66)$$

$$\frac{C_B}{N_b w_o} = \left[\frac{a^2 + b^2 + ab + abv(2a + 2b + abv)}{(1+av)^2(1+bv)^2} - \frac{1}{4} \right] v^2. \quad (67)$$

One can see from Eq. (65) that $G''_{a,b}(v) < 0$ for all finite v and hence exhibits a second-order phase transition at $\frac{1}{2} = G'_{a,b}(0)$, which gives the critical phase boundary on the a - b phase diagram: $4(a_c^2 + a_c b_c + b_c^2) = 1$, which is shown in the contour plot of the cost as a function of a and b in Fig. 8(a). The theoretical results are further verified by simulations for the measured mean connectivity as displayed in Fig. 8(b) showing perfect agreement with the analytic formula.

F. Hybrid phase transition

In some special situations, the optimized network undergoes a hybrid phase transition from the unconnected network to a network of finite (and not small) connectivity displaying an abrupt jump in \bar{A} but the emergence of nontrivial solution is not via the tangent bifurcation as in the case of first-order transition discussed in previous section. In fact, the emergence of the nontrivial solution resembles more the situation of the second-order transition with $G_{a,b}(0) > \frac{1}{2}$, but the nontrivial just emerged is always not small. Such a scenario results in a hybrid phase transition [20], exhibiting both first- and second-order characteristics. To illustrate the hybrid phase transition, here we consider the case of node and edge distributions p_{in} , p_{out} , and $p(w)$ are all uniformly distributed in $[0, 1)$. Relevant quantities such as $G_{a,b}(v)$, \bar{A} , and C_B can be derived analytically using Eqs. (39)–(41) to give

$$\bar{A} = \int_0^1 \int_0^1 dr ds f_w[(as + br)v], \quad f_w(z) = \begin{cases} 1, & z \geq 1 \\ z, & 0 < z < 1 \end{cases}, \quad (68)$$

$$\frac{C_B}{N_b w_o} = \frac{1}{2} \int_0^1 \int_0^1 dr ds \times \left(\begin{cases} 1, & (as + br)v \geq 1 \\ (as + br)^2 v^2, & (as + br)v < 1 \end{cases} - \frac{v^2}{4} \right), \quad (69)$$

where v is the root of the saddle-point equation

$$\frac{v}{2} = G_{a,b}(v) = \int_0^1 \int_0^1 dr ds (as + br) f_w[(as + br)v]. \quad (70)$$

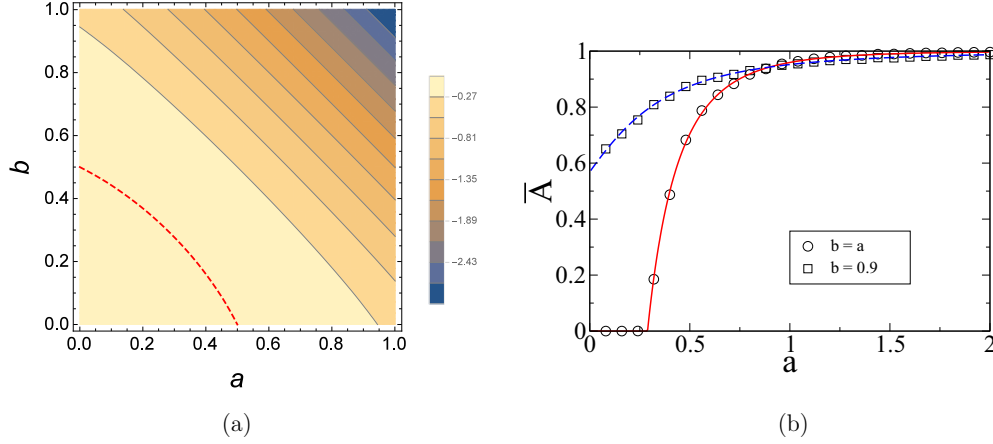


FIG. 8. Optimized directed network in Model B with nonnegative exponentially distributed inward and outward node weights, the nonnegative edge weight is also exponentially distributed. (a) Contour plot of the theoretical optimized cost (normalized) as a function of a and b . The critical phase boundary separating the optimized network to be unconnected or with finite connectivity, $4(a_c^2 + a_c b_c + b_c^2) = 1$, is also shown by the red dashed curve. (b) Simulation results of the optimized network for \bar{A} vs a the cases of $b = a$ and $b = 0.6$. The respective theoretical predictions from Eqs. (65) and (66) for \bar{A} are also shown.

In particular, $G_{a,b}(v) = \frac{v}{6}(2a^2 + 2b^2 + 3ab)$ for $v < 1/(a + b)$. The main feature that results in the hybrid phase transition can be traced to the properties in $G_{a,b}(v)$ having a finite region of linearity with positive slope for $v > 0$, as depicted in Fig. 9(a). If the slope is less than $\frac{1}{2}$, the trivial root is the only solution [dot-dashed curve in Fig. 9(a)]. The slope of the linear regime increases as the parameters vary and a nontrivial root of finite magnitude emerges for $G'_{a,b}(0) > \frac{1}{2}$ [solid curve in Fig. 9(a)] similar to the scenario of a second-order transition [see Fig. 4(a)], but here the difference is that the magnitude of the emerged root is not infinitesimally small even it is infinitesimally close into the finite connection phase. The hybrid phase transition boundary can be derived to be $2a^2 + 2b^2 + 3ab = 3$, which is shown in Fig. 9(b). The hybrid

phase boundary separates the unconnected network ($\bar{A} = 0$, lower left quadrant) from the optimized network of finite connectivity ($\bar{A} > 0$ and not small). Simulations are carried out to measure the \bar{A} of the optimized networks as a function of a for various values of b and the results (symbols) are plotted in Fig. 9(c), which are in perfect agreement with the corresponding theoretical results (curves).

V. OPTIMIZED NETWORK WITH NEGATIVE NODE-WEIGHTS

Here we consider the interesting situations in which some of the nodes can have negative node weights. A node with negative node weight means that the node does not favor

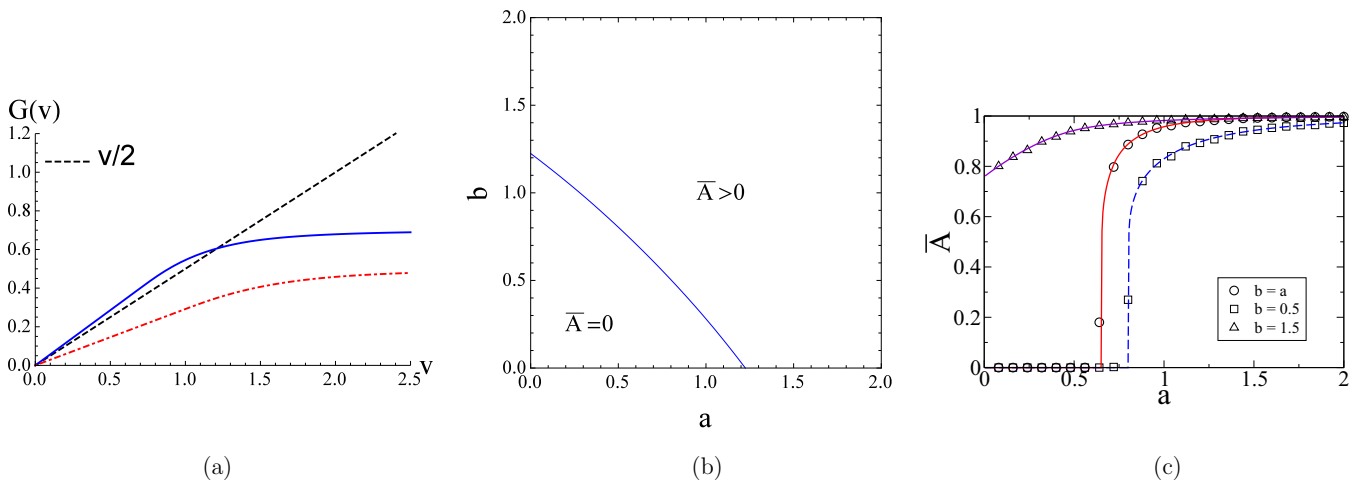


FIG. 9. Hybrid phase transitions in the directed Model B with node and edge weights follow the uniform distributions. (a) The function $G_{a,b}(v)$ for $2a^2 + 2b^2 + 3ab < 3$ (red dot-dashed curve) and $2a^2 + 2b^2 + 3ab > 3$ (blue solid curve). The $\frac{v}{2}$ line is also shown by the dashed line. (b) Phase diagram of b vs a . The hybrid phase boundary separating the unconnected network to optimized network with finite connectivity is denoted by the blue solid curve. (c) Simulation results for the optimized mean-connectivity as a function of a for various values of b . The simulation results (symbols) indicate a sharp jump in \bar{A} at $a = \sqrt{\frac{3}{7}} \simeq 0.65465$ for the case of $b = a$. The corresponding theoretical results (curves) are also shown.

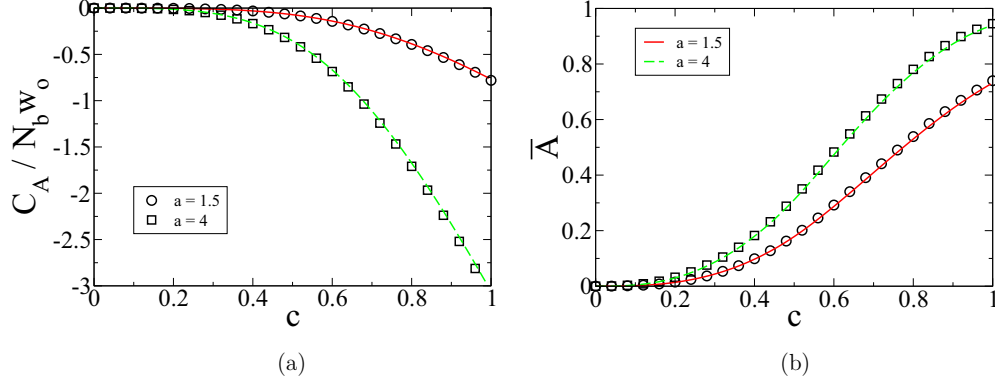


FIG. 10. Undirected optimized network of Model A with negative node weights with $p_\lambda(z)$ uniformly distributed in $z \in [c - 1, c]$, $0 < c < 1$ is the fraction of nodes with positive weights, and edge weight cumulative distribution $f_w(z) = (1 - e^{-z})\Theta(z)$. (a) The theoretical normalized cost as a function of c for fixed values of a as given by Eq. (72). $a = 1.5$ (solid red curve) and $a = 4$ (dashed green curve). (b) The optimized mean connectivity \bar{A} vs c for the cases in panel (a). Symbols are the simulation results and the curves are the theoretical results from Eq. (71).

for linking, and additional cost is needed to make a connection involving this node. If we think of a direct link as a kind of master-slave interaction in which the node with outward connection dominates over the node with inward connection, then optimizing the cost function can lead to richer properties. At first sight, if some nodes have large positive outward node weights while other nodes have large negative inward node weights, then this would result in strong frustration effects [21,22] that could induce a complex cost landscape that would impose additional challenge for the search of the fully optimized configuration [21–23]. Node with a large positive outward node weight and a large negative inward node weight might be destined to be a dominating outward hub in the optimized network. However, nodes with both large negative inward and outward node weights will tend to be isolated. In some situation, the interplay of the distributed positive and negative node weights in the system could result in clustering of nodes and community formation upon the optimization process. We will first examine the undirected optimized network models with negative node weight, which has not been investigated before in Refs. [13,14].

A. Undirected network with some nodes having negative node weights

For undirected network with positive or negative node weights, one can naturally classify the nodes into nodes with positive weights (denoted by \oplus) and nodes with negative weights (denoted by \ominus). For the case of Model A, since the node weights are nonnegative, Eq. (9) implies that there is no $\ominus - \ominus$ connection, and a higher chance for $\oplus - \oplus$ connections. This suggests the possibility of segregation of different node types or isolation of the \ominus nodes under certain conditions.

For explicit calculations, we first consider undirected network in Model A with uniformly distributed $P(\lambda) = 1/\lambda_o$ for $\lambda \in [\lambda' - \lambda_o, \lambda']$ where $\lambda_o > 0$ and $0 < \lambda' < \lambda_o$ so that the nodes have finite probabilities of having positive and negative weights. Using similar definitions as Eqs. (13) and (14), and defining $a \equiv \lambda_o/w_o$ for Model A as before and $c \equiv \lambda'/\lambda_o$, the scaled node weight distribution $p_\lambda(z)$ is uniformly distributed in $z \in [c - 1, c]$, and $0 < c < 1$ is the fraction of nodes with positive weights. The scaled edge weight cumulative distribution is $f_w(z) = (1 - e^{-z})\Theta(z)$. The mean connectivity can then be computed to give

$$\bar{A} = \begin{cases} -\frac{a^2(2c^2 - 4c + 1) - 2a(c - 1) + e^{-2ac} - 2e^{a-2ac} + 1}{a^2} & c \geq \frac{1}{2}, \\ \frac{2ac(ac - 1) - e^{-2ac} + 1}{a^2} & c < \frac{1}{2}, \end{cases} \quad (71)$$

$$\frac{C_A}{N_b w_o} = \begin{cases} -\frac{e^{-2ac} - 2e^{a-2ac} + 1}{a^2} + \frac{1}{3}a(4c^3 - 12c^2 + 6c - 1) + \frac{2(c-1)}{a} - 2c^2 + 4c - 1 & c \geq \frac{1}{2}, \\ \frac{1 - e^{-2ac}}{a^2} - \frac{4ac^3}{3} - \frac{2c}{a} + 2c^2 & c < \frac{1}{2}. \end{cases} \quad (72)$$

Figure 10(a) shows that the cost is always negative, keeps decreasing as a function of c , and is more negative for larger a . The simulation results for the mean connectivity are plotted in Fig. 10(b) showing that \bar{A} increases smoothly with c which agrees well with the theoretical results in Eq. (75).

For undirected network in Model B, Eq. (27) indicates that $\ominus - \ominus$ connections are equally favorable as the $\oplus - \oplus$ connections, but the $\oplus - \ominus$ connections are suppressed. This will induce segregation of the \oplus and \ominus nodes into two communities that are weakly linked. Again for explicit calculations, we consider undirected network in Model B also with $p_\lambda(z)$ uniformly distributed in $z \in [c - 1, c]$, $0 < c < 1$, the saddle-point equation reads

$$\frac{v}{2} = G_a(v) = a^2 \int_{c-1}^c \int_{c-1}^c dr ds (r + s)^2 f_w[av(r + s)], \quad (73)$$

and hence for edge distribution with $p(0) > 0$, a second-order phase transition occurs at $G'_a(0) = \frac{1}{2}$ giving the critical transition point at

$$a_c = \frac{1}{\sqrt{2p(0)[4c(c-1) + \frac{7}{6}]}}. \tag{74}$$

For $f_w(z) = (1 - e^{-z})\Theta(z)$, direct calculation after some algebra, one obtains the optimized mean connectivity

$$\bar{A} = \begin{cases} a[(K_{\square} - K_{LL})\Theta(v) + K_{LL}\Theta(-v)] & c \geq \frac{1}{2}, \\ a[K_{UR}\Theta(v) + (K_{\square} - K_{UR})\Theta(-v)] & c < \frac{1}{2} \end{cases}, \text{ where} \tag{75}$$

$$K_{\square} = 1 - \frac{(e^{av} - 1)^2 e^{-2acv}}{a^2 v^2}$$

$$K_{UR} = \frac{\eta(avc)}{a^2 v^2}, K_{LL} = \frac{\eta[av(c-1)]}{a^2 v^2}; \quad \eta(X) \equiv 2X(X-1) + 1 - e^{-2X}, \tag{76}$$

with v being the root of the saddle-point equation

$$\frac{v}{2} = G_a(v) = \begin{cases} a[(I_{\square} - I_{LL})\Theta(v) + I_{LL}\Theta(-v)] & c \geq \frac{1}{2}, \\ a[I_{UR}\Theta(v) + (I_{\square} - I_{UR})\Theta(-v)] & c < \frac{1}{2}, \end{cases} \text{ where} \tag{77}$$

$$I_{\square} = -\frac{2(e^{av} - 1)e^{-2acv}\{-acv + e^{av}[a(c-1)v + 1] - 1\}}{a^3 v^3} + 2c - 1 \tag{78}$$

$$I_{UR} = c^3 \phi(avc), I_{LL} = (c-1)^3 \phi[av(c-1)]; \quad \phi(X) \equiv \frac{4}{3} - \frac{2[X + e^{-2X}(X+1) - 1]}{X^3}. \tag{79}$$

The corresponding cost can be derived to give

$$\frac{C_B}{N_b w_o} = \begin{cases} a[(J_{\square} - J_{LL})\Theta(v) + J_{LL}\Theta(-v)] - \frac{v^2}{4} & c \geq \frac{1}{2}, \\ a[J_{UR}\Theta(v) + (J_{\square} - J_{UR})\Theta(-v)] - \frac{v^2}{4} & c < \frac{1}{2}, \end{cases} \text{ where} \tag{80}$$

$$J_{\square} = 1 - \frac{(e^{av} - 1)e^{-2acv}\{-2acv + e^{av}[2a(c-1)v + 3] - 3\}}{a^2 v^2}, \tag{81}$$

$$J_{UR} = \frac{\psi(avc)}{a^2 v^2}, J_{LL} = \frac{\psi[av(c-1)]}{a^2 v^2}; \quad \psi(X) \equiv 2(X-2)X - e^{-2X}(2X+3) + 3. \tag{82}$$

The second-order phase boundary can be derived to be

$$2[4c(c-1) + \frac{7}{6}] = a^2, \tag{83}$$

implying that a second-order transition occurs only for $a \leq \sqrt{\frac{13}{3}} \simeq 2.082$. The phase diagram with the second-order phase boundary is shown in Fig. 11(a). Notice that there is a reentrant phase transition for fixed $a < \sqrt{\frac{13}{3}}$ as c varies. Such a reentrant second-order phase transition is confirmed by simulation results of the optimized \bar{A} as shown in Fig. 11(b). In addition to the second-order transition, a first-order transition is possible as outlined by the following reasoning. Apart from the trivial $v = 0$ root, the saddle-point Eq. (77) has a positive root for $c > \frac{1}{2}$ if $G'(0^+) > \frac{1}{2}$. However, another negative root can coexist in some regime and the conditions can be deduced from Eq. (77) to be $a\partial_v I_{LL}|_{0^-} > \frac{1}{2}$, which gives $4a^2(1-c)^4 > 3/2$. Similar calculations for the case of $c < \frac{1}{2}$ leads to the condition of coexistence of positive and negative roots (denoted by $v^>$ and $v^<$, respectively) as $4a^2c^4 > 3/2$.

The coexistence of positive and negative roots is shown by the region bound by the dot-dashed curves in Fig. 11(a). In the coexistence region of $v^>$ and $v^<$, a first-order transition occurs at $c = \frac{1}{2}$ when $C_B(v^>) = C_B(v^<)$. Thus, there is a first-order transition for sufficiently large values of a , $a > \sqrt{6} \simeq 2.45$ as c varies across $c = \frac{1}{2}$ as marked by the dashed line in Fig. 11(a). Simulations are performed to measure the optimized \bar{A} for the first-order transition across $c = \frac{1}{2}$ and the results are shown in Fig. 11(b) (\square symbols), which agrees with the theoretical values. Although \bar{A} is continuous across $c = 1/2$, it is a first-order transition because the optimized cost C_B (the ‘‘free-energy’’) has a discontinuous derivative at $c = 1/2$.

B. Optimized directed network with negative node weights

For illustration, let us consider the case of exponential decay of edge weight distribution, but the inward node weights

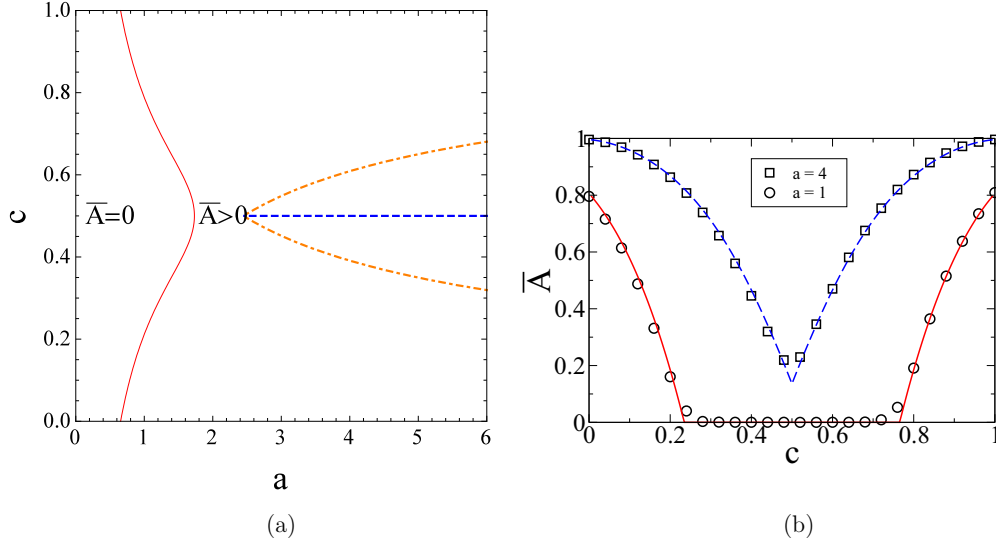


FIG. 11. Undirected optimized network of Model B with uniformly distributed node weights in $[c - 1, c]$, $0 < c < 1$. c is the fraction of nodes with positive weights. The edge weight cumulative distribution is $f_w(z) = (1 - e^{-z})\Theta(z)$. (a) Phase diagram of c vs a . The red curve is the second-order phase transition boundary given by Eq. (83) separating the unconnected network (left side) from the network with finite connections. The coexistence of positive and negative roots is shown by the region bound by the orange dot-dashed curves. The first-order transition is shown by the blue dashed line. (b) The optimized mean connectivity \bar{A} vs c for $a = 1$ (solid red curve) and $a = 4$ (dashed blue curve) showing the reentrant second-order phase transitions and first-order transition, respectively. Symbols are the simulation results and the curves are the theoretical results (75).

are nonpositive and the outward node weights are nonnegative which are also exponentially distributed, namely: $p_{\text{in}}(r) = e^r$, $r \in (-\infty, 0]$, $p_{\text{out}}(s) = e^{-s}$, $p(w) = e^{-w}$, where $r, s, w \in [0, \infty)$. Such a case can model the situation that nodes have a kind of dominating behavior that like to control (make outward connections to) others but not be influenced by others (having inward connections).

1. Model A

For the simpler case of Model A, direct calculations using Eqs. (16) and (17) give

$$\bar{A} = \frac{a^2}{(1+a)(a+b)}, \quad \frac{C_A}{N_b w_o} = -\frac{a^3}{(1+a)(a+b)}. \quad (84)$$

Figure 12(a) plots the normalized cost as a function of a for fixed value of b and the case of $b = a$, showing that the cost is always negative for finite values of a and decreases with a and b monotonically. Simulation results for the optimized mean connectivity are plotted in Fig. 12(b). Notice that for the case of $b = a$, i.e., the inward and outward node weights are opposite but of same magnitude on average, $\bar{A} < \frac{1}{2}$ and only approach to the upper bound of $\frac{1}{2}$ when $b = a \rightarrow \infty$. The theoretical results of \bar{A} from Eq. (84) are also displayed showing perfect agreement.

2. Model B: First-order transition due to positive-negative node symmetry and reentrant transition

Before we investigate the phase transition properties, let us examine the possibility of a spin-glass phase due to the apparent frustration in this case of both ferro and antiferromagnetic spin-spin coupling. Notice that the Hamiltonian (28) is of the

form of a Mattis spin glass [24] and the spin-spin coupling term can be rewritten as $\sum_{\gamma\rho} |\Lambda_\gamma| |\Lambda_\rho| \text{sgn}(\Lambda_\gamma) \text{sgn}(\Lambda_\rho) S_\gamma S_\rho$, where sgn is the sign function that takes the value of 1 or -1 . Thus, by redefining $S_\gamma \rightarrow \text{sgn}(\Lambda_\gamma) S_\gamma$, the apparent frustration can be gauged away. Hence, there is no frustration and no spin-glass phase even if Λ 's can be negative. This fact can also be reflected from the fact that the cost landscapes are not complex [as revealed in Figs. 15(a) and 15(b)]. However, if there are some additional constraints or penalty on establishing the connections, then frustrations can actually occur, as in the case of two-dimensional networks with edge crossing penalty which can induce antiferromagnetic coupling [15].

The nature of the phase transitions in this case can be revealed from Eqs. (39)–(41). After some algebra, one can derive

$$\frac{v}{2} = G_{a,b}(v) = \frac{a^3 v(2+av)}{(a+b)(1+av)^2} \Theta(v) + \frac{b^3 v(2-bv)}{(a+b)(1-bv)^2} \Theta(-v), \quad (85)$$

$$\bar{A} = \frac{v}{a+b} \left[\frac{a^2}{(av+1)} \Theta(v) + \frac{b^2}{(bv-1)} \Theta(-v) \right], \quad (86)$$

$$\frac{C_B}{N_b w_o} = \left[\frac{a^3}{(av+1)^2} \Theta(v) + \frac{b^3}{(bv-1)^2} \Theta(-v) \right] \times \frac{v^2}{a+b} - \frac{v^2}{4}. \quad (87)$$

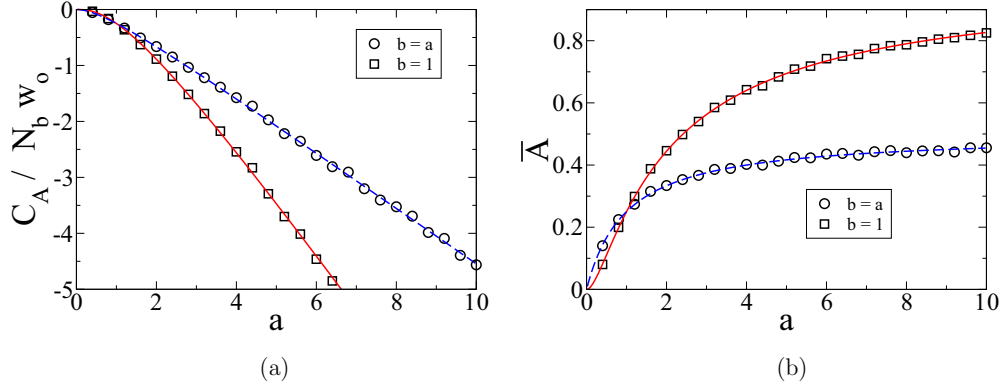


FIG. 12. Optimized directed network in Model A with exponentially distributed negative inward node weights and exponentially distributed positive outward node weights, the nonnegative edge weight is also exponentially distributed. (a) The theoretical normalized cost as a function of a for $b = a$ (dashed blue curve) and $b = 1$ (solid red curve). (b) The optimized mean connectivity \bar{A} vs a for the cases in panel (a). Symbols are the simulation results and the curves are the theoretical results from Eq. (84).

The saddle-point equation (85) is quadratic and can be solved explicitly to give a positive ($v^>$) or negative ($v^<$) root:

$$v = \begin{cases} v^> \equiv \frac{4a^3 - a - b}{a[a + b - a^3 + a\sqrt{a(2a + 2b + a^3)}]} & \text{if } 4a^3 - a - b > 0, \\ v^< \equiv -\frac{4b^3 - a - b}{b[a + b - b^3 + b\sqrt{b(2a + 2b + b^3)}]} & \text{if } 4b^3 - a - b < 0. \end{cases} \quad (88)$$

Only the trivial $v = 0$ exists (the optimized network is unconnected with $\bar{A} = 0$) in the region of $4a^3 - a - b < 0$ and $4b^3 - a - b > 0$ [the lower left region in the phase diagram Fig. 13(a)]. A second-order phase transition occurs across the critical phase boundaries of $4a^3 - a - b = 0$ and $4b^3 - a - b = 0$, which is qualitatively similar to the case of positive inward node weights in Fig. 8. However, for the present case with negative inward node weights, a new the coexistence ($v^>$ and $v^<$ coexist) regime appears in the $4a^3 - a - b > 0$

and $4b^3 - a - b < 0$ regime [the upper right region in the phase diagram Fig. 13(a)]. In the coexistence regime, the optimized solution is determined by the roots with the lower cost which is exchanged as one crosses the positive-negative node symmetry (i.e., $b = a$) line. As demonstrated in Fig. 13(b) for increasing a with b fixed at $b = 1$, the lowest cost root switched from the $v^<$ branch to the $v^>$ branch as a crosses the $a = b$ boundary and the optimized v (recall $v = \bar{A}$) shows an abrupt jump characterising a first-order transition. Detail examination of the theoretical phase diagram further reveals the existence of reentrant (i.e., $v = 0 \rightarrow v \neq 0 \rightarrow v = 0$ along some path in the phase diagram) second-order phase transitions, for example for any fixed value of $b \in (\frac{1}{2}, \frac{1}{\sqrt{2}})$, as a increases from 0, reentrant phase transition occurs across the two different second-order phase boundaries.

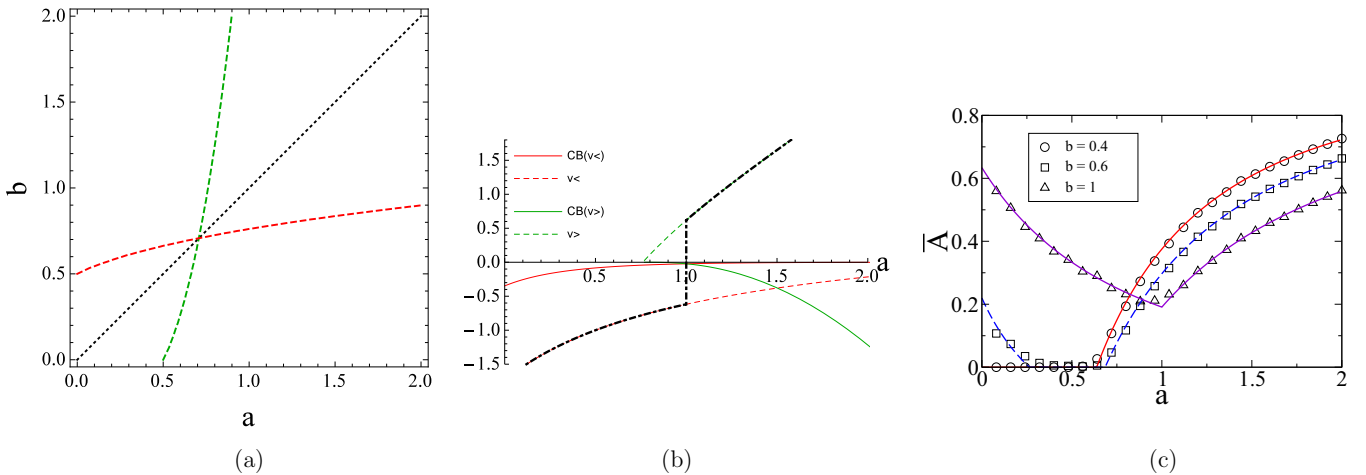


FIG. 13. Optimized directed network in Model B with exponentially distributed negative inward node weights and exponentially distributed positive outward node weights, the nonnegative edge weight is also exponentially distributed. (a) Phase diagram of b vs a showing the boundary of second-order phase transitions given by $4a^3 = a + b$ (the green dashed curve) and $4b^3 = a + b$ (the red dashed curve). The first-order phase boundary of $b = a$ is shown by the black dotted line. (b) Nontrivial roots of the saddle-point equation (85) plotted as a function of a for $b = 1$. The positive and negative roots together with the corresponding normalized cost are also shown. The black dot-dashed curve denoted the optimized solution with the lowest cost, showing a jump at $a = b$ signifying a first-order transition. (c) Simulation results of the optimized network for \bar{A} vs a for the cases of $b = 0.4$, $b = 0.6$ and $b = 1$ showing, respectively, the second-order, reentrant, and first-order phase transitions. The respective theoretical predictions from Eqs. (85) and (86) for \bar{A} are also shown.

The above theoretical results are verified by the simulation results of the measured mean-connectivity of the optimized network as a function of a for various fixed values of b . As shown in Fig. 13(c), \bar{A} shows the characteristic behavior of second-order, reentrant, and first-order phase transitions, respectively, for fixed values of $b = 0.4$, $b = 0.6$, and $b = 1$.

VI. OPTIMAL COST ALGORITHM FOR DIRECTED NETWORKS AND COST FUNCTION IN ORDERED SPACE

For the simpler case of Model A, the optimized network connections are simply given by Eq. (9). For a given local node weights of λ^{in} and λ^{out} , one simply make the connection when $\lambda^{\text{in}} + \lambda^{\text{out}}$ exceeds the correspond edge weight w in the simulations.

As for Model B with nonnegative node weights, the zero-temperature local mean-field equations can be used to find the optimized network configuration. In principle, the coupled nonlinear equations (37) can be solved numerically to find all possible solution and the one with the lowest C_B can then be selected. But such an approach is inefficient as the number of equations is $N_b = N(N - 1)$ can be rather large (e.g., $N_b = 249\,500$ for a network of $N = 500$ nodes). Here we can extend the zero-temperature algorithm developed for the undirected networks [13] to the case for directed connections, and further develop efficient algorithm to handle the case with negative node weights.

A. Algorithm for nonnegative node weights

Exploiting the zero-temperature mean-field equation (37), one can develop an algorithm to find the optimized network configuration efficiently, similar to the case of undirected networks. For a given realization of the edge weights $\{w_\gamma\}$, and sum of inward and outward edge weights $\{\Lambda_\gamma\}$ (recall $\Lambda_\gamma \equiv \Lambda_{ij} = \lambda_i^{\text{in}} + \lambda_j^{\text{out}}$ for the $j \rightarrow i$ connection), we first set $A_\gamma = 0$ if $\Lambda_\gamma = 0$ which follows from Eq. (37) for nonnegative w_γ . Then for those nonzero Λ_γ , one defines the sequence $\Omega_\gamma \equiv w_\gamma / \Lambda_\gamma$ and sort it in increasing order to form the ordered sequence $\{\Omega_{\tilde{\gamma}}\}$, where the ordered sequence index is denoted with a $\tilde{\gamma}$. Then locate all the ‘local minima’ along the sorted sequence, i.e., find the values of $\tilde{\mu}$ satisfying

$$\Omega_{\tilde{\mu}+1} \geq \frac{2}{N_b} \sum_{\tilde{\sigma}}^{\tilde{\mu}} \Lambda_{\tilde{\sigma}} > \Omega_{\tilde{\mu}}. \tag{89}$$

A candidate for the optimized solution is

$$A_{\tilde{\sigma}} = \begin{cases} 1 & \text{for } \tilde{\sigma} = 1, \dots, \tilde{\mu}, \\ 0 & \text{for } \tilde{\sigma} = \tilde{\mu} + 1, \dots, N_b. \end{cases} \tag{90}$$

The corresponding cost and mean connectivity can be easily evaluated to be

$$C_B(\tilde{\mu}) = \sum_{\tilde{\gamma}=1}^{\tilde{\mu}} w_{\tilde{\gamma}} - \left(\frac{1}{N} \sum_{\tilde{\gamma}=1}^{\tilde{\mu}} \Lambda_{\tilde{\gamma}} \right)^2, \tag{91}$$

$$\bar{A} = \frac{\tilde{\mu}}{N_b}. \tag{92}$$

Finally, the costs of all the $\tilde{\mu}$ candidates together with that of zero connection and fully connected networks are compared,

and the final optimized solution is the one with the lowest cost. The same method has been applied in previous studies of undirected network with nonnegative node weights and proved to be much more efficient as compared to the traditional Monte Carlo simulation method by annealing to low temperatures [13]. The key reason for the high efficiency of our algorithm is that the solution space dramatically reduce from the search in 2^{N_b} configuration states to the ordered index space of $N_b + 1$ states. For $N = 500$, this amounts to a reduction from $2^{24950} \simeq 5 \times 10^{7510}$ down to 24 951 states.

The insights obtained from the above results suggest that one can analyze the network optimization problem in the ordered index space using the expression (91), which can in general be obtained straightforwardly for given edge and node weights realization. In some special scenarios, the functional dependence of $C_B(\tilde{\mu})$ can be derived theoretically using order statistics [25], which will be illustrated below for several cases of homogeneous inward and outward node weights, i.e., $P_{\text{in}}(\lambda) = \delta(\lambda - \lambda_o^{\text{in}})$ and $P_{\text{out}}(\lambda) = \delta(\lambda - \lambda_o^{\text{out}})$. Under such conditions, the second term on the right-hand side (rhs) of Eq. (91) can be trivially evaluated. Furthermore, the ordering of Ω_γ will simply be the same as ordering the edge weights w_γ , and thus the expectation of the first term on the rhs of Eq. (91) can be evaluated for a given $P(w)$. Consider for example $P(w)$ is uniformly distributed in $[0, w_o]$, using order statistics, one obtains for $N_b \gg 1$,

$$\frac{C_B(\tilde{\mu})}{N_b w_o} = \left(\frac{1}{2} - (a + b)^2 \right) \left(\frac{\tilde{\mu}}{N_b} \right)^2. \tag{93}$$

The explicit expression of $C_B(\tilde{\mu})$ can be conveniently analyzed further to reveal the phase transition properties of the optimized network as follows. It is easy to see from Eq. (93) that $\tilde{\mu} = 0$ is the global cost minimum if $a + b < \frac{1}{\sqrt{2}}$, but for $a + b > \frac{1}{\sqrt{2}}$ the global minimum jumps to $\tilde{\mu} = N_b$, signifying a first-order transition from the unconnected network to a fully connected network at $a + b = \frac{1}{\sqrt{2}}$. Figure 14(a) plots the normalized $C_B(\tilde{\mu})$ for the cases of $a + b < \frac{1}{\sqrt{2}}$ and $a + b > \frac{1}{\sqrt{2}}$.

Another example is $P(w) = \frac{1}{w_o} \exp(-\frac{w}{w_o})$ $w \in [0, \infty)$, after some calculations, one gets

$$\frac{C_B(\tilde{\mu})}{N_b w_o} = \frac{\tilde{\mu}}{N_b} + \left(1 - \frac{\tilde{\mu}}{N_b} \right) [H_{N_b - \tilde{\mu}} - H_{N_b}] - (a + b)^2 \left(\frac{\tilde{\mu}}{N_b} \right)^2 \tag{94}$$

$$= \frac{\tilde{\mu}}{N_b} + \left(1 - \frac{\tilde{\mu}}{N_b} \right) \ln \left(1 - \frac{\tilde{\mu}}{N_b} \right) - (a + b)^2 \left(\frac{\tilde{\mu}}{N_b} \right)^2 \tag{95}$$

for $N_b \gg 1$,

where $H_m \equiv \sum_{k=1}^m \frac{1}{k}$ is the harmonic number. Taking derivatives of $C_B(\tilde{\mu})$, one easily finds that $\tilde{\mu} = 0$ is always an extremum for the cost, indicating that the unconnected network is always a solution of the mean-field equations. In addition, since $\frac{C_B''(0)}{N_b w_o} = 1 - 2(a + b)^2$, the $\tilde{\mu} = 0$ state is the global minimum of the cost only if $a + b < \frac{1}{\sqrt{2}}$, and another (global) minimum with a negative cost emerges for $a + b > \frac{1}{\sqrt{2}}$ signifying a second-order phase. These results are in agreement with that of Fig. 6(a), but is more straightforward

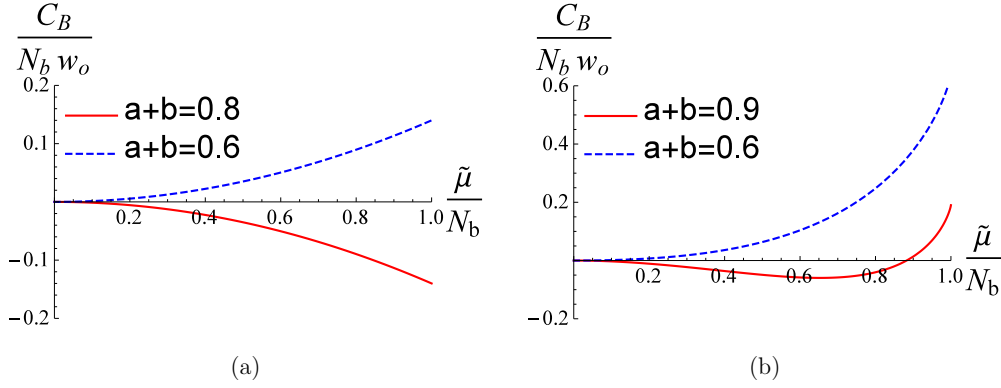


FIG. 14. (a) Theoretical result of the normalized cost as a function of the normalized sorted index $\frac{\tilde{\mu}}{N_b}$ with $P(w)$ uniformly distributed in $[0, w_o]$, $P_{\text{in}}(\lambda) = \delta(\lambda - \lambda_o^{\text{in}})$, and $P_{\text{out}}(\lambda) = \delta(\lambda - \lambda_o^{\text{out}})$. (b) Similar to panel (a) but with $P(w) = \frac{1}{w_o} \exp(-\frac{w}{w_o})$.

and intuitive using Eq. (95). Figure 14(b) plots the normalized $C_B(\tilde{\mu})$ for the cases of $a + b < \frac{1}{\sqrt{2}}$ and $a + b < \frac{1}{\sqrt{2}}$.

B. Modified algorithm for negative node weights

For the directed network Model B, if some nodes has negative node weights (either inward or outward), then some edges can have $\Lambda_\gamma < 0$. According to Eq. (37), the condition to make a connection becomes $\Omega_\gamma \equiv w_\gamma / \Lambda_\gamma > 2\bar{\Lambda}A$. Thus, instead of sorting Ω_γ in an increasing order, Ω_γ needs to be sorted in decreasing order for $\Lambda_\gamma < 0$. Hence, one creates two sorted sequences, one for $\Lambda_\gamma > 0$, and the other for $\Lambda_\gamma < 0$. The local minima for these two sorted sequences, $\tilde{\mu}$ and $\tilde{\nu}$, are located according to the following rules:

$$\begin{cases} \Omega_{\tilde{\mu}+1} \geq \frac{2}{N_b} \sum_{\tilde{\sigma}=1}^{\tilde{\mu}} \Lambda_{\tilde{\sigma}} > \Omega_{\tilde{\mu}}, & \Lambda_{\tilde{\sigma}} > 0, \\ \Omega_{\tilde{\nu}+1} \leq \frac{2}{N_b} \sum_{\tilde{\sigma}'=1}^{\tilde{\nu}} \Lambda_{\tilde{\sigma}'} < \Omega_{\tilde{\nu}}, & \Lambda_{\tilde{\sigma}'} < 0, \end{cases} \quad (96)$$

where the sorted indices $\tilde{\sigma}$ is for nonnegative Λ 's and $\tilde{\rho}$ is for the negative ones. After finding all $\tilde{\mu}$ and $\tilde{\nu}$ that satisfy the inequalities (96), then compare all the solutions (including the trivial ones) to select the lowest cost one for the optimized solution.

The corresponding cost and mean connectivity can be easily evaluated to be

$$\begin{aligned} C_B(\tilde{\mu}, \tilde{\nu}) &= \sum_{\tilde{\sigma}=1, \tilde{\sigma} \in \Lambda^+}^{\tilde{\mu}} w_{\tilde{\sigma}} + \sum_{\tilde{\rho}=1, \tilde{\rho} \in \Lambda^-}^{\tilde{\nu}} w_{\tilde{\rho}} \\ &\quad - \left(\frac{1}{N} \sum_{\tilde{\sigma}=1, \tilde{\sigma} \in \Lambda^+}^{\tilde{\mu}} \Lambda_{\tilde{\sigma}} + \frac{1}{N} \sum_{\tilde{\rho}=1, \tilde{\rho} \in \Lambda^-}^{\tilde{\nu}} \Lambda_{\tilde{\rho}} \right)^2, \end{aligned} \quad (97)$$

$$\bar{A} = \frac{\tilde{\mu} + \tilde{\nu}}{N_b}. \quad (98)$$

The properties of the optimized network can be conveniently obtained by analyzing the cost function given by Eq. (97) using the minimization principle in the two-dimensional ordered index space. For illustrative purpose, consider the case of homogeneous negative inward and positive outward node

weights, i.e., $P_{\text{in}}(\lambda) = \delta(\lambda + \lambda_o^{\text{in}})$ and $P_{\text{out}}(\lambda) = \delta(\lambda - \lambda_o^{\text{out}})$, whose functional dependence of $C_B(\tilde{\mu}, \tilde{\nu})$ can also be derived theoretically using order statistics [25]. For $P(w)$ uniformly distributed in $[0, w_o]$, one obtains for $N_b \gg 1$,

$$\begin{aligned} \frac{C_B(\tilde{\mu}, \tilde{\nu})}{N_b w_o} &= \frac{1}{2} \left[\left(\frac{\tilde{\mu}}{N_b} \right)^2 + \left(\frac{\tilde{\nu}}{N_b} \right)^2 \right] - (b - a)^2 \left(\frac{\tilde{\mu} + \tilde{\nu}}{N_b} \right)^2, \\ &\quad \times \frac{\tilde{\mu}}{N_b} + \frac{\tilde{\nu}}{N_b} \leq 1. \end{aligned} \quad (99)$$

Figure 15(a) shows the contour plot of the normalized cost $C_B(\tilde{\mu}, \tilde{\nu})$ in Eq. (99) for $a \equiv \frac{\lambda_o^{\text{out}}}{\sqrt{w_o}} = 1.48$ in which $(0,0)$ is the stable global minimum and hence the unconnected network is the trivial optimized state. However, for $b \equiv \frac{\lambda_o^{\text{in}}}{\sqrt{w_o}} = 1$ as shown in Fig. 15(b), $(0,0)$ becomes a saddle and the global minimum shifts to $(\frac{1}{2}, \frac{1}{2})$ and the optimized state is the fully connected network. From Eq. (99), it is easy to verify that $(\frac{\tilde{\mu}}{N_b}, \frac{\tilde{\nu}}{N_b}) = (0, 0)$ is the only local extremum. The stability of $(0,0)$ can be directly obtained from the eigenvalues of the Jacobian, which can be calculated to be 1 and $1 - 4(b - a)^2$. Thus, the $(0,0)$ state (unconnected network) has the minimal cost for $|b - a| < \frac{1}{2}$, but becomes unstable (a saddle) when $|b - a| > \frac{1}{2}$. Furthermore, the eigenvector associated with the unstable eigenvalue of $1 - 4(b - a)^2$ is along the $(1,1)$ direction and flows to the global minimum of $(\frac{1}{2}, \frac{1}{2})$ (and hence $\bar{A} = 1$, the fully connected network) which is the edge of the allow domain in Fig. 15(b). The above simple analysis reveals the first-order transition with the phase boundary given by $|b - a| = \frac{1}{2}$ separating the unconnected optimized network and the fully connected optimized network. Simulations are performed to find the optimized network and the mean connectivity is plotted as a function of a for various values of b , as shown in Fig. 15(d). As predicted by the above theoretical analysis, a first-order transition is observed, and reentrant first-order transitions occur in some parameter regime as predicted from the theoretical phase diagram. For instance, reentrant phase transition occurs for a fixed value of $b > \frac{1}{2}$ as a increases, as revealed from the phase diagram

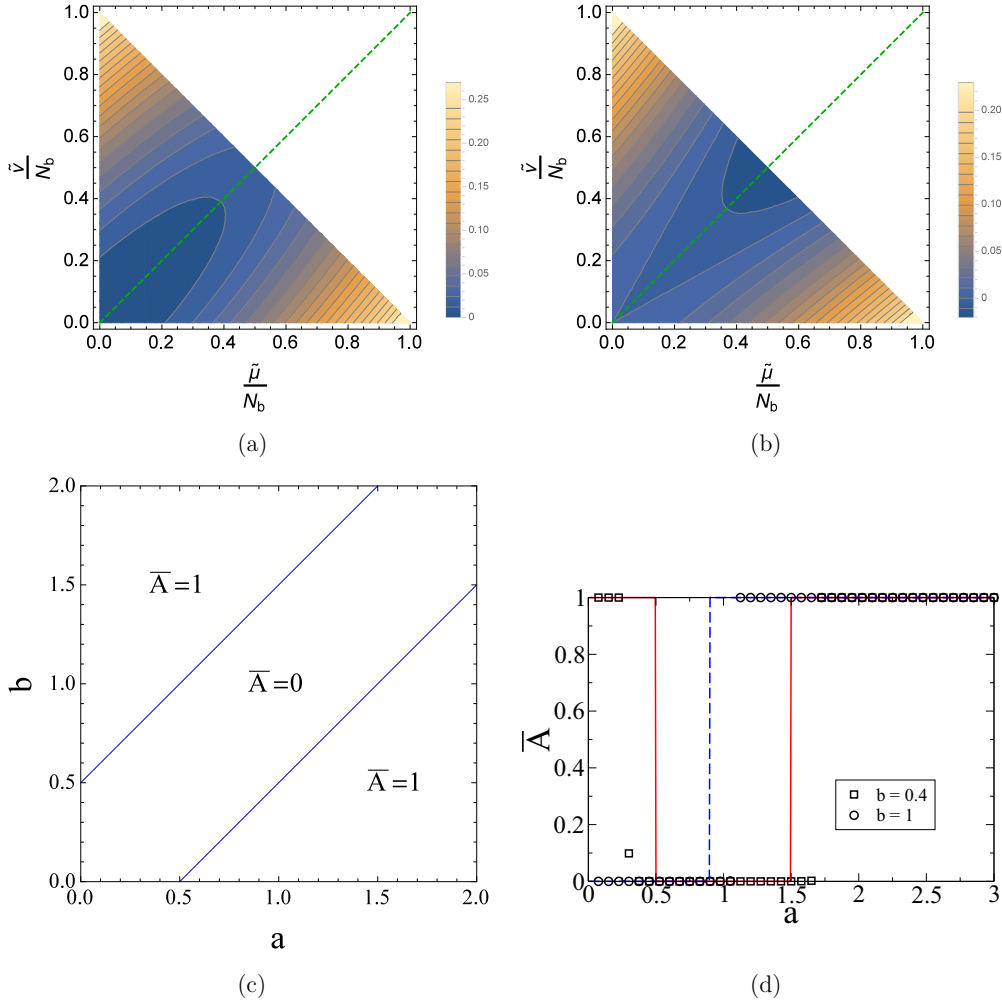


FIG. 15. Contour plot of the theoretical normalized cost as a function of $\frac{\bar{\mu}}{N_b}$ and $\frac{\bar{\nu}}{N_b}$ for $P(w)$ uniformly distributed in $[0, w_o]$, $P_{in}(\lambda) = \delta(\lambda + \lambda_o^{in})$ and $P_{out}(\lambda) = \delta(\lambda - \lambda_o^{out})$ for : (a) $a \equiv \frac{\lambda_o^{out}}{\sqrt{w_o}} = 1.48$ and $b \equiv \frac{\lambda_o^{in}}{\sqrt{w_o}} = 1$. (0,0) is the stable global minimum, (b) $a = 1.52$ and $b = 1$. (0,0) becomes a saddle and the global minimum becomes $(\frac{1}{2}, \frac{1}{2})$. (c) Phase diagram showing the region of the first-order phase transition boundaries separating the unconnected network with $\bar{A} = 0$ (the central diagonal stripe region) and the fully connected optimized network with $\bar{A} = 1$. (d) Simulation results of the measured \bar{A} of the optimized network as a function of a for $b = 0.4$ and $b = 1$. The theoretical results are shown by solid and dashed curves.

Fig. 15(c), which is also confirmed by the simulation results of the optimized \bar{A} shown in Fig. 15(d) for $b = 1$.

VII. SUMMARY AND OUTLOOK

In this work, we considered the growth of the directed links in network models that aim at minimizing the connection expenses while at the same time favoring other important network properties such as network connections. Our motivation is to understand the relation between the energy cost and the connectivity in a network. These models are quite general and can be applicable in various physical or biological networks. By generalizing the recently studied optimization of undirected network connection models, a similar mapping of the directed network model to an Ising spin model can also be achieved and analyzed by employing statistical mechanics methods. It is found that the models under studied can be solved exactly or analytical results can be derived for general edge, inward and outward node weights that are distributed

independently. These models exhibit a variety of interesting phase transition behavior in many scenarios, signifying abrupt changes in the network structures. Our Model A is relatively simple and demonstrates that the directed network model can be mapped to an Ising spin system under a local external field in which exact results can be obtained. Its ground-state solution can be found straightforwardly by placing a directed link if its weight w_α is less than the corresponding sum of inward and outward node weights, Λ_α .

However, Model B involves edge interactions which is less trivial. In Model B, the network model is mapped to Ising spins with infinite-range interactions and hence can be precisely described by the mean-field theory. Using the mean-field equations and with appropriate extensions, we also obtain an efficient algorithm for finding the fully optimized directed network configuration as in the case of undirected optimized networks. Traditional metropolis Monte Carlo simulations can explore efficiently the phase space and perform well only for temperatures that are not too low. However,

our algorithm applies well for the search of the fully optimized zero-temperature case in which traditional Monte Carlo method will be frozen and become ineffective. This algorithm is efficient because it drastically reduces the search configuration space and also provides further insights in terms of the cost function in ordered space. Monte Carlo simulations are carried out explicitly using the efficient algorithm to confirming the validity of our theoretical results, and the efficiency of our algorithm.

In addition, the scenarios with negative node weights in optimized network models, which have not studied previously even for the undirected network, were also considered in this work. The possibility of segregation of nodes and clustering can be analyzed in detail, thus providing insights for the plausible mechanisms in network community formation as a result of network optimization. Efficient simulation algorithm to include the case of negative node weights to search for the fully optimized zero-temperature configuration were also developed and employed to verify the corresponding theoretical results.

A wide class of interesting phase transitions, including first-order, second-order, and hybrid ones, is obtained in the framework of our models. The change near the second-order transition point from the unconnected to network with sparse connections can provide some insights for the nature of many realistic networks which are found to be sparse. However, the drastic change from finite connectivity to an unconnected network across a first-order transition may capture the abrupt failure of network linkage or communication in the breakdown of network or grid structures.

In this paper, we focused on the phase transitions associated with the optimized directed network models. After the network is optimized with the lowest total cost, the properties in the optimized network can then be further analyzed theoretically and also be measured by simulations, which will be presented in a future publication. Key features of the fully optimized directed network, such as degree distributions, cluster coefficients, minimal path lengths, key motifs occurrence, etc. will provide valuable information on the properties of the optimized network, as well as for further identification of the edge and node weights in the present model in terms of the parameters in realistic physical or biological networks. For example, if one takes the positive node weights as the local firing rate of a neuron, then the node weights can enhance the internode connection if $\Lambda_{ij} = \lambda_i^{\text{in}} + \lambda_j^{\text{out}}$ is sufficiently large,

which can be interpreted as a rough version of the Hebb's rule of "firing enhances wiring" [26].

The directed network optimized connection problem in the presence of additional constraints, such as strong inter-link topological interactions [27] as in the case of entangled polymer chains [28–30]. The edge crossing penalty in two-dimensional networks [15], would enhance the complexity for the search of the fully optimized configuration. Only undirected network with unweighted nodes were investigated for the optimization of two-dimensional networks with edge crossing penalty or forbiddance in Ref. [15], it is of interest to investigate the optimization of directed two-dimensional network with heterogeneous node of positive and negative inward or outward node weights and probe the optimized network structures.

In general, the question of what kind of weight and node distributions used will produce the given observed optimized weight and degree distributions is a challenging inverse problem that is under investigation. An even more ambitious goal is to uncover the evolution principle, presumably governed by some optimization model, from the observed network structure. This is an even more challenging inverse problem of inferring the cost function and its parameters from the observed links such as the optimized w_α . Such a task is difficult because often the network connection weights and directions are not directly available in practice, and usually only the dynamical data of network nodes can be observed. Therefore, one first needs to infer the network structure from the time-series data of the nodes. Then with the increasing availability of dynamical data of network nodes, together with several recently proposed reliable and efficient methods for the reconstruction of networks from the time-series dynamics data of the nodes [31–40] that can be employed. Such an approach should be promising with the suitable implementation of network reconstruction schemes and the inference of optimization model from network structure to be developed. Hopefully it can open a new avenue of deducing the network evolution principle, which is usually a long time scale process, from the relatively short observation times in the node dynamics.

ACKNOWLEDGMENT

This work has been supported by the National Science and Technology Council of Taiwan under Grant No. 110-2112-M-008-026-MY3.

-
- [1] Nature, Special issue on Big Data **455**, No. 7209 (2008).
 - [2] M. E. J. Newman, The structure and function of complex networks, *SIAM Rev.* **45**, 167 (2003).
 - [3] M. E. J. Newman, *Networks: An Introduction* (Oxford University Press, Oxford, UK, 2010).
 - [4] A. E. Motter and Z. Toroczkai, Introduction: Optimization in networks, *Chaos* **17**, 026101 (2007).
 - [5] B. Li and K. Y. Michael Wong, Optimizing synchronization stability of the Kuramoto model in complex networks and power grids, *Phys. Rev. E* **95**, 012207 (2017).
 - [6] H. Ronellenfisch and E. Katifori, Global Optimization, Local Adaptation, and the Role of Growth in Distribution Networks, *Phys. Rev. Lett.* **117**, 138301 (2016).
 - [7] J.-Y. Huang, C.-W. Huang, K.-C. Kao, and P.-Y. Lai, Robustness and adaptation reveal plausible cell cycle controlling subnetwork in *Saccharomyces cerevisiae*, *Gene* **518**, 35 (2013).
 - [8] E. Bullmore and O. Sporns, The economy of brain network organization, *Nat. Rev. Neurosci.* **13**, 336 (2012).

- [9] G. Tkačik, A. M. Walczak, and W. Bialek, Optimizing information flow in small genetic networks, *Phys. Rev. E* **80**, 031920 (2009).
- [10] A. M. Walczak, G. Tkačik, and W. Bialek, Optimizing information flow in small genetic networks. II. Feed-forward interactions, *Phys. Rev. E* **81**, 041905 (2010).
- [11] T. Tanizawa, G. Paul, R. Cohen, S. Havlin, and H. E. Stanley, Optimization of network robustness to waves of targeted and random attacks, *Phys. Rev. E* **71**, 047101 (2005).
- [12] T. P. Peixoto and S. Bornholdt, Evolution of Robust Network Topologies: Emergence of Central Backbones, *Phys. Rev. Lett.* **109**, 118703 (2012).
- [13] A.-L. Cheng and P.-Y. Lai, Phase transitions in optimized network models, *J. Stat. Mech.* (2020) 093404.
- [14] A.-L. Cheng and P.-Y. Lai, Optimized network properties in network growing models, *Chin. J. Phys.* **77**, 411 (2022).
- [15] A.-L. Cheng and P.-Y. Lai, Optimized two-dimensional networks with edge-crossing cost: Frustrated antiferromagnetic spin system, *Phys. Rev. E* **104**, 054313 (2021).
- [16] S. N. Dorogovtsev, A. V. Goltsev, and J. F. F. Mendes, Critical phenomena in complex networks, *Rev. Mod. Phys.* **80**, 1275 (2008).
- [17] G. Palla, Imre Derényi, Illés Farkas, and Tamás Vicsek, Statistical mechanics of topological phase transitions in networks, *Phys. Rev. E* **69**, 046117 (2004).
- [18] S. Thurner and C. Biely, Two statistical mechanics aspects of complex networks, *Physica A* **372**, 346 (2006).
- [19] D. J. Thouless, P. W. Anderson, and R. G. Palmer, Solution of “solvable model of a spin glass,” *Philos. Mag.* **35**, 593 (1977).
- [20] G. J. Baxter, S. N. Dorogovtsev, K.-E. Lee, J. F. F. Mendes, and A. V. Goltsev, Critical Dynamics of the k -Core Pruning Process, *Phys. Rev. X* **5**, 031017 (2015).
- [21] K. Binder and A. P. Young, Spin glasses: Experimental facts, theoretical concepts, and open questions, *Rev. Mod. Phys.* **58**, 801 (1986).
- [22] P. Y. Lai and Y. Y. Goldschmidt, Application of statistical mechanics to combinatorial optimization problems: The chromatic number problem and q -partitioning of a graph, *J. Stat. Phys.* **48**, 513 (1987).
- [23] Y. Y. Goldschmidt and P. Y. Lai, q -partitioning of graphs with finite coordination number, *J. Phys. A: Math. Gen.* **21**, L1043 (1988).
- [24] D. C. Mattis, Solvable spin systems with random interactions, *Phys. Lett. A* **56**, 421 (1976).
- [25] H. A. David and H. N. Nagaraja, *Order Statistics* (Wiley, New York, 2003).
- [26] D. O. Hebb, *The Organization of Behavior* (Wiley, New York, 1949).
- [27] M. Doi and S. F. Edwards, *Theory of Polymer Dynamics* (Oxford University Press, Oxford, UK, 1986).
- [28] Y.-J. Sheng, P.-Y. Lai, and H.-K. Tsao, Nonequilibrium relaxation of a stretched polymer chain, *Phys. Rev. E* **56**, 1900 (1997).
- [29] Y.-J. Sheng, P.-Y. Lai, and H.-K. Tsao, Topological effects on statics and dynamics of knotted polymers, *Phys. Rev. E* **58**, R1222 (1998).
- [30] J.-Y. Huang and P.-Y. Lai, Crossings and writhe of flexible and ideal knots, *Phys. Rev. E* **63**, 021506 (2001).
- [31] E. S. C. Ching, P.-Y. Lai, and C. Y. Leung, Extracting connectivity from dynamics of networks with uniform bidirectional coupling, *Phys. Rev. E* **88**, 042817 (2013).
- [32] H. Song, C.-C. Chen, J.-J. Sun, P.-Y. Lai, and C. K. Chan, Reconstruction of network structures from repeating spike patterns in simulated bursting dynamics, *Phys. Rev. E* **90**, 012703 (2014).
- [33] E. S. C. Ching, P.-Y. Lai, and C. Y. Leung, Reconstructing weighted networks from dynamics, *Phys. Rev. E* **91**, 030801 (2015).
- [34] Z. Zhang, Z. Zheng, H. Niu, Y. Mi, S. Wu, and G. Hu, Solving the inverse problem of noise-driven dynamic networks, *Phys. Rev. E* **91**, 012814 (2015).
- [35] E. S. C. Ching and H. C. Tam, Reconstructing links in directed networks from noisy dynamics, *Phys. Rev. E* **95**, 010301 (2017).
- [36] P.-Y. Lai, Reconstructing network topology and coupling strengths in directed networks of discrete-time dynamics, *Phys. Rev. E* **95**, 022311 (2017).
- [37] H. C. Tam, E. S. C. Ching, and P.-Y. Lai, Reconstructing networks from dynamics with correlated noise, *Physica A* **502**, 106 (2018).
- [38] F. Goetze and P.-Y. Lai, Reconstructing positive and negative couplings in Ising spin networks by sorted local transfer entropy, *Phys. Rev. E* **100**, 012121 (2019).
- [39] C. Sun, K. C. Lin, C. Y. Yeung, E. S. C. Ching, Y.-T. Huang, P.-Y. Lai, and C. K. Chan, Revealing directed effective connectivity of cortical neuronal networks from measurements, *Phys. Rev. E* **105**, 044406 (2022).
- [40] C.-H. Cheng and P.-Y. Lai, Efficient reconstruction of directed networks from noisy dynamics using stochastic force inference, *Phys. Rev. E* **106**, 034302 (2022).